

**Optical-  
microphysical  
properties of Saharan  
dust aerosols**

A. Papayannis et al.

**Optical-microphysical properties of  
Saharan dust aerosols and composition  
relationship using a multi-wavelength  
Raman lidar, in situ sensors and  
modelling: a case study analysis**

**A. Papayannis<sup>1</sup>, R. E. Mamouri<sup>1</sup>, V. Amiridis<sup>2</sup>, E. Remoundaki<sup>3</sup>, G. Tsaknakis<sup>1</sup>,  
P. Kokkalis<sup>1</sup>, I. Veselovskii<sup>4</sup>, A. Kolgotin<sup>4</sup>, A. Nenes<sup>5,6</sup>, and C. Fountoukis<sup>6</sup>**

<sup>1</sup>National Technical University of Athens, Laser Remote Sensing Laboratory, Zografou, Greece

<sup>2</sup>National Observatory of Athens, Institute for Space Applications and Remote Sensing, Athens, Greece

<sup>3</sup>National Technical University of Athens, School of Mining and Metallurgical Engineering, Zografou, Greece

<sup>4</sup>Physics Instrumentation Center for General Physics, Troitsk, 142190 Moscow, Russia

<sup>5</sup>Georgia Inst. of Tech., School of Earth and Atmos. Sc. and Chem. & Biomolecular Engineering, Atlanta GA, USA

<sup>6</sup>Institute of Chemical Engineering and High Temperature Chemical Processes, Foundation for Research and Technology Hellas (FORTH), Patras, Greece

25473

Title Page

Abstract

Introduction

Conclusions

References

Tables

Figures

⏪

⏩

◀

▶

Back

Close

Full Screen / Esc

Printer-friendly Version

Interactive Discussion



Received: 11 July 2011 – Accepted: 2 September 2011 – Published: 12 September 2011

Correspondence to: A. Papayannis (apdlidar@central.ntua.gr)

Published by Copernicus Publications on behalf of the European Geosciences Union.

ACPD

11, 25473–25516, 2011

---

**Optical-  
microphysical  
properties of Saharan  
dust aerosols**

A. Papayannis et al.

---

Title Page

Abstract

Introduction

Conclusions

References

Tables

Figures



Back

Close

Full Screen / Esc

Printer-friendly Version

Interactive Discussion

## Abstract

A strong Saharan dust event occurred over the city of Athens, Greece (37.9° N, 23.6° E) between 27 March and 3 April 2009. The BSC-DREAM8b model was used to forecast the dust event and to provide the vertical profiles of the aerosol concentration. Due to mixture of dust particles with low clouds during most of the reported period, the dust event could be followed by the National Technical University of Athens (NTUA) 6-wavelength Raman lidar system only during the unclouded day of 2 April 2009. The lidar data obtained were used to retrieve the vertical profile of the optical (extinction and backscatter coefficients) properties of aerosols in the troposphere. Additionally, a retrieval technique representing dust as a mixture of spheres and spheroids was used to derive the mean aerosol dust microphysical properties (mean and effective radius, number, surface and volume density, and mean refractive index) in different layers between 1.8 and 3.5 km a.s.l. The final data set of the aerosol optical and microphysical properties along with the water vapor profiles obtained by Raman lidar were incorporated into the ISORROPIA II model to infer an in situ aerosol composition consistent with the retrieved refractive index values. PM<sub>10</sub> concentrations levels, PM<sub>10</sub> composition results and SEM-EDX (Scanning Electron Microscope-Energy Dispersive X-ray) analysis results on sizes and mineralogy of particles from samples during the Saharan dust transport event were used to evaluate the retrieval.

## 1 Introduction

Atmospheric aerosols have a large impact on the planetary radiation budget, and are thought to exert a net cooling effect on climate (Andreae, 1995; Ramanathan et al., 2001; Heinold et al., 2007; Levin and Cotton, 2009; Ramanathan and Feng, 2009; Lohmann et al., 2010). The cooling effect associated with anthropogenic aerosol is thought to partially mitigate greenhouse gas warming, but estimates are highly uncertain, owing to the large spatiotemporal variability of aerosol and their complex

## Optical- microphysical properties of Saharan dust aerosols

A. Papayannis et al.

Title Page

Abstract

Introduction

Conclusions

References

Tables

Figures

⏪

⏩

◀

▶

Back

Close

Full Screen / Esc

Printer-friendly Version

Interactive Discussion



interaction with atmospheric constituents, radiation and clouds (Forster et al., 2007). Mineral dust is an important component of the atmospheric aerosol loading, as it accounts for about 75 % of the global aerosol mass load and 25 % of the global aerosol optical depth (Kinne et al., 2006), as well as a key player in earth's radiative transfer budget (Mahowald et al., 2006) affecting precipitation (Yoshioka et al., 2007). Northern Africa (Sahara desert and Sahel), Saudi Arabia, and Eastern Asia (Taklemakan and Gobi deserts) are the main source regions of dust around the globe (Marticorena et al., 1997; Laurent et al., 2008). According to simulations by Laurent et al. (2008), the largest dust emissions originate from the Sahara (which for 1996 to 2001 range between 585 and 759 Tgyr<sup>-1</sup>) exhibit marked seasonal cycles (with a maximum in summer for the Western Sahara and in spring for the eastern Sahara) and pronounced interannual variability. This implies a highly complex and uncertain radiative forcing pattern, which is exacerbated by variability in dust optical properties from atmospheric processing and fluctuations in dust mineralogy (e.g. clay content, Helmert et al., 2007). Dust impacts on regional climate, precipitation (Min et al., 2009), public health (Annesi-Maesano et al., 2007) and transportation (Satheesh et al., 2005; Heinold et al., 2007) can be even more important. For example, Ganor et al. (2010) reported on an increasing trend of dust days over Israel (average rate of 2.7 days per decade), with important climatic implications for the Mediterranean and Europe in general.

Lidar aerosol measurements of dust optical properties and atmospheric vertical distribution can provide much of the information required to constrain models and reduce uncertainties associated with radiative forcing estimates. Towards this, the European Aerosol Research Lidar Network (EARLINET; <http://www.earlinet.org>) since 2000 provides the first systematic aerosol lidar observations of Saharan dust aerosols over the European continent, on a coherent network basis (Ansmann et al., 2003; Papayannis et al., 2008). A detailed lidar-derived climatology of dust layer heights, aerosol backscatter, lidar ratio (LR) and aerosol optical depth (AOD) values over Europe is provided by Papayannis et al. (2008). Moreover, the lidar technique has been extensively used from ground to provide the aerosol optical (e.g. Ansmann et al., 2003; Blanco et

**Optical-  
microphysical  
properties of Saharan  
dust aerosols**

A. Papayannis et al.

Title Page

Abstract

Introduction

Conclusions

References

Tables

Figures

⏪

⏩

◀

▶

Back

Close

Full Screen / Esc

Printer-friendly Version

Interactive Discussion



al., 2003; Balis et al., 2004; Papayannis et al., 2008; Santese et al., 2008; Tesche et al., 2009), geometrical (Mattis et al., 2008), hygroscopic (Feingold and Morley, 2003) and microphysical (Müller et al., 1999, 2005; Pahlow et al., 2006; Müller et al., 2009b, 2010) properties, as well as to measure cloud condensation nuclei (CCN) (Feingold et al., 1998; Ghan and Collins, 2004) in the atmosphere, and also from space (e.g. Berthier et al., 2006; Mamouri et al., 2009; Liu et al., 2011).

This study focuses on the optical, microphysical and composition of aged dust aerosol particles associated with a strong Saharan dust event as they interact with anthropogenic particles in the lower free troposphere over an urban site (Athens, Greece). In the following sections we first present the dust forecasting model, instrumentation and methodology used for retrieving the aerosol properties (Sect. 2). An analysis of the dust event then follows (Sect. 3) with an emphasis on the days with optimal lidar retrievals. We then conclude (Sect. 4) with final remarks and a summary.

## 2 Methodology

### 2.1 The NTUA 6-wavelength Raman lidar system

The National Technical University of Athens (NTUA) lidar system is located on Campus in the city of Athens (37.97° N, 23.79° E, 200 m above sea level-a.s.l.), and has been continuously operating since the initiation of the EARLINET project (Bösenberg et al., 2003) in February 2000. The compact 6-wavelength NTUA Raman lidar system (Mamouri et al., 2008) is based on a pulsed Nd:YAG laser emitting simultaneously at 355, 532 and 1064 nm. The lidar signals are detected at six wavelengths 355, 387, 407, 532, 607 and 1064 nm. The system has been quality-assured by performing direct inter-comparisons, both at hardware (Matthias et al., 2004a) and software levels (Böckmann et al., 2004; Pappalardo et al., 2004).

To obtain reliable and quantitative lidar aerosol retrievals, several techniques and methods have to be combined. The standard backscatter lidar technique is appropriate

## Optical- microphysical properties of Saharan dust aerosols

A. Papayannis et al.

Title Page

Abstract

Introduction

Conclusions

References

Tables

Figures



Back

Close

Full Screen / Esc

Printer-friendly Version

Interactive Discussion



---

**Optical-  
microphysical  
properties of Saharan  
dust aerosols**A. Papayannis et al.

---

[Title Page](#)[Abstract](#)[Introduction](#)[Conclusions](#)[References](#)[Tables](#)[Figures](#)[⏪](#)[⏩](#)[◀](#)[▶](#)[Back](#)[Close](#)[Full Screen / Esc](#)[Printer-friendly Version](#)[Interactive Discussion](#)

to retrieve aerosol parameters mostly for small aerosol optical depths ( $AOD < 0.2$ – $0.3$  in the visible), assuming a reference height in an aerosol-free area (e.g. the upper troposphere). Under such conditions, the Klett inversion technique (Klett, 1985) is used to retrieve the vertical profile of the aerosol backscatter coefficient ( $b_{aer}$ ) at the respective wavelengths. The resulting average uncertainty on the retrieval of  $b_{aer}$  (including both statistical and systematic errors corresponding to a 30–60 min averaging time) in the troposphere is of the order of 20–30 % (Bösenberg et al., 1997). To overcome the large uncertainty associated with this technique, the Raman  $N_2$  lidar technique was adopted using the methodology of Ansmann et al. (1992). Since the Raman lidar signals are quite weak, the Raman technique is mostly used during nighttime, when the atmospheric background is quite low.

In the case of the Raman technique, the measurement of the elastic backscatter signals at 355 and 532 nm, as well as that of the  $N_2$  inelastic-backscatter signals at 387 and 607 nm, respectively, permits the determination of the extinction ( $a_{aer}$ ) and backscatter ( $b_{aer}$ ) coefficients independently of each other (Ansmann et al., 1992) and, thus, of the extinction-to-backscatter ratio, the so-called lidar ratio (LR) at both wavelengths (355 and 532 nm). The uncertainties associated with the retrieved  $b_{aer}$  vertical profiles are of the order of 10–15 % (Mattis et al., 2002). The vertical profiles of  $b_{aer}$  referring to measurements performed before the local sunset time ( $\sim 19:00$  UT) were retrieved by using the Klett technique, using a LR value derived for dust aerosols by the Raman technique (Ansmann et al., 1992) from the same day's nighttime lidar measurements.

## 2.2 The CIMEL sunphotometer

The sunphotometric observations reported in this paper were performed by a CIMEL sun-sky radiometer (Holben et al., 1998), which is part of the Aerosol Robotic Network (AERONET) Global Network (<http://aeronet.gsfc.nasa.gov>). The instrument is located on the roof of the Research Center for Atmospheric Physics and Climatology of the Academy of Athens ( $37.99^\circ$  N,  $23.78^\circ$  E, elevation: 130 m). The site is located in the

city center and 10 km from the sea. This sunphotometric station is operated by the Institute for Space Applications and Remote Sensing (ISARS) of the National Observatory of Athens (NOA). The CIMEL data used in this study will provide information about the columnar AOD, aerosol size distribution, aerosol microphysical properties, and Ångström exponent. The AERONET data products along with the technical specifications of the CIMEL instrument are given in detail in Holben et al. (1998).

### 2.3 The MODIS instrument

The Moderate Resolution Imaging Spectroradiometer (MODIS) was launched in December 1999 on the polar orbiting Terra spacecraft and since February 2000 has been acquiring daily global data in 36 spectral bands from the visible to the thermal infrared (29 spectral bands with 1 km, 5 spectral bands with 500 m, and 2 spectral bands with 250 m nadir pixel dimensions). The MODIS aerosol products are only created for cloud-free regions. The atmospheric optical depth (AOD) values are retrieved by MODIS at 550 nm (<http://modis-atmos.gsfc.nasa.gov/products.html>) for both oceans (best) and land (corrected) (Tanré et al., 1997; Levy et al., 2007). The main sources of uncertainty in the retrieval of the AOD in this case are from instrument calibration errors, cloud-masking errors, incorrect assumptions on surface reflectance and aerosol model (fine (with radius  $\ll 1 \mu\text{m}$ ) and coarse (with radius  $\gg 1 \mu\text{m}$ ) mode aerosol models) selection (Remer et al., 2005; Levy et al., 2010). Therefore, selection of an inappropriate aerosol model can result in systematic AOD errors. The pre-launch conditions suggested that 1 standard deviation of retrievals would fall within  $\pm(0.03 + 0.05 \tau)$  over ocean and  $\pm(0.05 + 0.15 \tau)$  over land, where  $\tau$  is the AOD. These error bounds, derived pre-launch, are referred to as the expected error (EE) (Remer et al., 2005).

To minimize the uncertainties on the MODIS AOD product several validation studies have been performed, during pre-launch and post-launch procedures regarding the AOD measurements using ground-based instrumentation (Chu et al., 2003; Remer et al., 2005; Misra et al., 2008; Papadimas et al., 2009; Prasad and Singh, 2009). More recently, Levy et al. (2010) performed a global evaluation of the MODIS Collection 5

**Optical-  
microphysical  
properties of Saharan  
dust aerosols**

A. Papayannis et al.

Title Page

Abstract

Introduction

Conclusions

References

Tables

Figures



Back

Close

Full Screen / Esc

Printer-friendly Version

Interactive Discussion



---

## Optical- microphysical properties of Saharan dust aerosols

A. Papayannis et al.

---

[Title Page](#)[Abstract](#)[Introduction](#)[Conclusions](#)[References](#)[Tables](#)[Figures](#)[Back](#)[Close](#)[Full Screen / Esc](#)[Printer-friendly Version](#)[Interactive Discussion](#)

(C005) dark-target aerosol products over land, showing that that >66% (one standard deviation) of MODIS-retrieved AOD values compared to AERONET observed values within an expected error (EE) envelope of  $\pm(0.05 + 15\%)$ , with high correlation ( $R = 0.9$ ). According to the same authors, Terra's global AOD bias changes with time, underestimating by  $\sim 0.005$ , after the year 2004. However, although validated globally, MODIS-retrieved AOD does not fall within the EE envelope in all regions of the planet (Levy et al., 2010).

In this study we used MODIS C005 data, which were recently evaluated and validated for the Greater Mediterranean Basin ( $29.5^\circ\text{N}$ – $46.5^\circ\text{N}$  and  $10.5^\circ\text{W}$ – $38.5^\circ\text{E}$ ) against 29 AERONET stations, as described by Papadimas et al. (2009), who found that when comparing C005 to C004 data, the correlation coefficient increases from 0.66 to 0.76, and the slope of the linear regression fit from 0.79 to 0.85 whereas the offset decreased from 0.12 to 0.04 and the scatter of compared data pairs from 0.15 to 0.12. On the other hand, they found a significant decrease of AOD values over land (by 25.8%) for AODs > 0.2. However, the MODIS C005 data still overestimate/underestimate the AERONET AOD values smaller/larger than 0.25, but to a much smaller extent than C004 data.

### 2.4 The BSC-DREAM8b dust model

The updated version of the Dust Regional Atmospheric Model (BSC-DREAM8b) (Nickovic et al., 2001; Pérez et al., 2006a, b; Jiménez-Guerrero et al., 2008) has been delivering operational dust forecasts over the North Africa-Mediterranean-Middle East and over Asia regions on the last years at the Barcelona Supercomputing Center (BSC) (currently at [www.bsc.es/projects/earthscience/DREAM/](http://www.bsc.es/projects/earthscience/DREAM/)). The model simulates or predicts the 3-dimensional field of the dust concentration in the troposphere. The dust model takes into account all major processes of dust life cycle, such as dust production, horizontal and vertical diffusion and advection and wet and dry deposition, while the chemical aging and aerosol-cloud interactions are not taken into account. The model also includes the effects of the particle size distribution on aerosol dispersion.

The model numerically solves the Euler-type mass partial differential equation by integrating it spatially and temporally. The dust production is parameterized using near surface turbulence and stability, as well as soil features. The dust production mechanism is based on viscous/turbulent mixing close to the surface and soil moisture content.

In BSC-DREAM8b the aerosol description is improved from 4 to 8 bins (8 particle size categories with radii from 0.1 to 38  $\mu\text{m}$ ) and dust-radiation interactions are included (Haustein et al., 2009). For the present study, BSC-DREAM8b simulation is initialized with 24-hourly (at 00:00 UTC) updated NCEP (National Centers for Environmental Prediction)  $0.5^\circ \times 0.5^\circ$  analysis data and the initial state of the dust concentration in the model is defined by the 24-h forecast from the previous-day model run (because there are not yet satisfactory three-dimensional dust concentration observations to be assimilated). The resolution is set to  $1/3^\circ$  ( $\sim 50$  km) in the horizontal and to 24 layers extending up to approximately 15 km in the vertical. For long-range transport dust studies, only the particles with radii from 0.1 to 10  $\mu\text{m}$  are considered, since their lifetime is larger than about 12 h.

## 2.5 Derivation of the aerosol microphysical and chemical properties using models

The measured vertical profiles of the aerosol backscatter and extinction coefficients at multiple wavelengths can be inverted for particle microphysical parameter profiles using the regularization technique (Müller et al., 1999; Veselovskii et al., 2002, 2009). However, an application of this technique to dust needs to account for their nonsphericity, given that backscattering by irregularly shaped particles is weaker than by equivalent-volume spheres (Mishchenko et al., 2000). To address this issue, Mishchenko et al. (1997) suggested approximating the dust particles with a mixture of polydisperse, randomly oriented spheroids, as they can mimic the aerosol optical properties. Dubovik et al. (2006) have recently included the spheroid model in the AERONET retrieval algorithm, while Merikallio et al. (2011) studied the applicability of spheroidal model particles for simulating the single-scattering optical properties of mineral dust aerosols.

## Optical-microphysical properties of Saharan dust aerosols

A. Papayannis et al.

Title Page

Abstract

Introduction

Conclusions

References

Tables

Figures

⏪

⏩

◀

▶

Back

Close

Full Screen / Esc

Printer-friendly Version

Interactive Discussion



---

## Optical- microphysical properties of Saharan dust aerosols

A. Papayannis et al.

---

Title Page

Abstract

Introduction

Conclusions

References

Tables

Figures

⏪

⏩

◀

▶

Back

Close

Full Screen / Esc

Printer-friendly Version

Interactive Discussion



Veselovskii et al. (2010) introduced the spheroid model into the lidar retrieval of dust particles physical properties, by assuming that aerosols are a mixture of spheres and randomly oriented spheroids with a size-independent shape distribution. This assumption is applied to all particles. However, we must keep in mind that for the fine mode the optical properties of spheres and spheroids are very close and real difference occurs only for the coarse mode. Besides, the result is not very sensitive to the exact type of shape distribution. Thus, the assumption of size-independent shape proposed here remains quite reasonable. Moreover, our numerical simulations demonstrate that for 10 % uncertainty of input optical data (backscatter and extinction coefficients) the dust particle volume density and the effective radius can be estimated to within 30 %.

In this paper the microphysical properties of the aerosols in the lower free troposphere, inside the dust layer, were retrieved using the regularization technique (Veselovskii et al., 2002, 2004, 2010), which used as input the vertical profiles of the aerosol extinction  $a_{\text{aer}}$  (at 355–532 nm) and backscatter coefficients  $b_{\text{aer}}$  (at 355–532–1064 nm) retrieved from the elastic and Raman backscattered lidar signals (obtained at 5 different wavelengths: 355–387–532–607–1064 nm). The aerosol microphysical properties inverted concern the effective radius ( $r_{\text{eff}}$ ), the total number ( $N$ ), the surface area ( $S$ ) and volume ( $V$ ), as well as the real and imaginary part of the particle refractive index ( $m_{\text{R}}$  and  $m_{\text{i}}$ , respectively), in different layers in the lower troposphere (1.8–3.5 km height a.s.l.). In our approach we do not consider the spectral dependence of the refractive index size, nor the chemical composition of the aerosol particles. Thus, the retrieved values of the refractive index are the mean ones with respect to the size and spectral range considered (355–1064 nm). Additionally, in our retrieval we consider the real part of the refractive index ( $m_{\text{R}}$ ) to be in the range 1.33–1.65 and the aerosol particles diameters in the range between 0.075 and 20  $\mu\text{m}$ . The uncertainty on the  $m_{\text{R}}$  and  $m_{\text{i}}$  retrieval is of the order of  $\pm 0.05$  and  $\pm 0.0035$ , respectively, while the corresponding uncertainty of the retrieved values of the effective radius, volume and surface density is about  $\pm 30\%$ . Finally, the uncertainty on the number density estimation is about 50 % (Veselovskii et al., 2010).

---

**Optical-  
microphysical  
properties of Saharan  
dust aerosols**A. Papayannis et al.

---

[Title Page](#)[Abstract](#)[Introduction](#)[Conclusions](#)[References](#)[Tables](#)[Figures](#)[⏪](#)[⏩](#)[◀](#)[▶](#)[Back](#)[Close](#)[Full Screen / Esc](#)[Printer-friendly Version](#)[Interactive Discussion](#)

We have to clarify here that the inverse problem (using lidar data to retrieve the aerosol micro-physical properties) in our formulation is underdetermined: the set of lidar measurements is limited to 5 different wavelengths. Unfortunately, this is not sufficient to uniquely describe the properties of the aerosol. Therefore, we use an intermediate approach whose detailed description is given by Veselovskii et al. (2010). In our case we identify not a unique solution but a family of solutions instead. At the same time, in this process of identifying a family of solutions we use a priori constraints, thus we specifically limit the range of the considered values of the aerosol refractive index. Although those constraints do not provide uniqueness of the solution they significantly help to reduce the number of solution family members. Once the solution family is identified the results are averaged and the mean solution is provided. Thus in our approach we do not use a priori information about a certain particle size distribution (PSD) type, but we assume the size distribution ranging already mentioned before (0.075 to 20  $\mu\text{m}$ ). At the same time, the retrieved PSD is characterized by significant uncertainty, as it is shown will be shown later (e.g. Fig. 7b).

The inverted refractive index (which corresponds to in-situ conditions, i.e. includes aerosol water) along with the water vapor profiles obtained by Raman lidar over Athens and the temperature and relative humidity profiles obtained by radiosonde, were incorporated in the thermodynamic model ISORROPIA II (Fountoukis and Nenes, 2007) to infer the composition. The model treats the thermodynamics of aerosol containing K, Ca, Mg,  $\text{NH}_3/\text{NH}_4$ , Na,  $\text{SO}_4/\text{HSO}_4$ ,  $\text{HNO}_3/\text{NO}_3$ , HCl/Cl and  $\text{H}_2\text{O}$ . ISORROPIA-II can predict composition for the “stable” (or deliquescent path) solution where salts precipitate once the aqueous phase becomes saturated with respect to a salt, and, a “metastable” solution, where the aerosol is composed only of an aqueous phase regardless of its saturation state. ISORROPIA-II was executed in “reverse” mode, where known quantities are T, RH and the concentrations of aerosol K, Ca, Mg,  $\text{NH}_4$ , Na,  $\text{SO}_4$ ,  $\text{NO}_3$  and Cl. The output provided by ISORROPIA-II is the aerosol phase state (solid only, solid/aqueous mixture or aqueous only) and the speciation in the gas and aerosol phases. The model has been evaluated with ambient data from a wide

range of environments (including “dust-rich”) (Moya et al., 2001; Zhang et al., 2003; San Martini et al., 2006; Nowak et al., 2006; Metzger et al., 2006; Fountoukis et al., 2009), while its computational rigor and performance makes it suitable for use in large scale air quality and chemical transport models. Some examples of such 3-D models that have implemented ISORROPIA-II are GISS, CMAQ, PMCAM<sub>x</sub>, GEOS-Chem, and ECHAM/MESSy (Adams and Seinfeld, 2002; Yu et al., 2005; Pye et al., 2009; Karydis et al., 2010; Pringle et al., 2010).

In order to use ISORROPIA in combination with the Raman lidar data, an assumption concerning the aerosol composition has to be done, mainly due to the absence of air mass sample within the under study layers. In our procedure, at first a typical composition of sulfate, ammonium sulfate and mineral dust aerosols was considered. ISORROPIA was run forward for the computation of complex refractive index for each aerosol composition, using as input the relative humidity and the temperature within an aerosol layer. Finally, the aerosol composition (a mixture of sulfate, ammonium and mineral dust) with the closest refractive index (both real and imaginary part) value to the one estimated by the inversion model is provided as the most acceptable composition value.

## 2.6 In situ measurements of aerosol properties

In situ sampling of dust aerosols mixed with urban-like ones was performed to infer the mass concentration and the composition of dust particles near ground. The sampling site was installed at the NTUA Campus at the top of a building at 14 m height from ground level (located 200 m above the mean sea level) and included: PM<sub>10</sub> continuous concentration monitoring by TSI Dustrak 8520 and TCR TECORA aerosol sampling. The sampling procedure and the elemental composition determinations are described in detail in Remoundaki et al. (2011).

Briefly, PM<sub>10</sub> sampling for elemental composition determination and SEM-EDX (Scanning Electron Microscope-Energy Dispersive X-ray) analysis was carried out using a TCR TECORA (Sentinel PM) operating at 38.33 l min<sup>-1</sup>, constructed and

25484

ACPD

11, 25473–25516, 2011

## Optical- microphysical properties of Saharan dust aerosols

A. Papayannis et al.

Title Page

Abstract

Introduction

Conclusions

References

Tables

Figures

⏪

⏩

◀

▶

Back

Close

Full Screen / Esc

Printer-friendly Version

Interactive Discussion



calibrated in order to comply with European Standard EN12341 for standard sampling of PM<sub>10</sub>. The sampling device operates with autonomy of 16 samples charged in a charging cassette by programming the sampling span and duration. Aerosol samples were collected on 0.45 μm nuclepore membranes. Twelve samples have been collected from 27 March to 2 April 2009. From 28 March to 2 April, two 3-h samples per day were collected: one starting 06:00 UTC and the second starting at 11:00 UTC in order to correspond to urban activities maxima. This 3-h time span during the two urban activities maxima (beginning and end of working day) was also selected in order to avoid sampling interruption due to filter clogging.

Sampling material and filter keeping petri-dishes were pretreated by soaking in dilute nitric acid solution and thorough rinsing by ultra-pure water (18 MΩcm<sup>-1</sup>) and dried under the laminar flow hood of the laboratory. In order to determine PM<sub>10</sub> concentrations, the nuclepore membranes were weighted before and after sampling according to the procedure described in Annex C of EN12341 (EN12341, 1999) using a Mettler Toledo MS105 with a resolution of 10 μg in the air conditioned weighing room of the laboratory. The pre-weighted membranes were charged to the filter supports and sampler cassette under the laminar flow hood. Filter blanks and blank field samples were also prepared and analyzed together with samples. The filters were also weighted according to the same procedure as described before. The elemental composition determinations have been carried out by EDXRF (SPECTRO XEPOS bench top XRF spectrometer SPECTRO A.I. GmbH) with Pd end window X-ray tube. NIST standard SRM 2783 has been used for spectrometer calibration verification. The elements Si, Al, Fe, K, Ca, Mg, S, Ni, Cu, Zn, Mn, and Ti, have been determined. SPECTRO X-LAB PRO was used for values normalization and error correction. The method detection limits were 100 ng cm<sup>-2</sup> for Mg, 20 ng cm<sup>-2</sup> for Al and K, 10 ng cm<sup>-2</sup> for Ca, Ti, Fe, 5 ng cm<sup>-2</sup> for Si, Mn, 2 ng cm<sup>-2</sup> for Ni, 1 ng cm<sup>-2</sup> for S, Cu and Zn. The estimated precision of the method ranged between 0.1 % and 30 % for individual elements, for most of them being <5 %.

**Optical-  
microphysical  
properties of Saharan  
dust aerosols**

A. Papayannis et al.

Title Page

Abstract

Introduction

Conclusions

References

Tables

Figures

⏪

⏩

◀

▶

Back

Close

Full Screen / Esc

Printer-friendly Version

Interactive Discussion



### 3 Case study: 27 March–3 April 2009 dust episode

This case study concerns an intense Saharan dust outbreak, which lasted for eight days (27 March to 3 April 2009) and affected most of the Eastern Mediterranean and Balkans. The ground and remote sensing instruments were operated continuously during this period (although the NTUA Raman lidar was operated during the end of the episode, when clouds were dispersed and aerosol optical depths were low enough to permit sampling by the laser beam. MODIS and CIMEL instruments did not provide aerosol optical depth between 29 March and 1 April, due to extensive cloud cover.

Figure 1 presents the BSC-DREAM8b predictions of total dust in size classes between 0.1 and 10  $\mu\text{m}$  (in  $\text{g m}^{-2}$ ) over the European continent at 12:00 UTC. Superimposed on the same figure are the corresponding hourly forecasted wind vectors at 3000 m height level. From this figure we see that during the studied period Athens is influenced by high values of dust loadings (up to 1.5  $\text{g m}^{-2}$ ) from 29 March to 3 April. These large amounts of dust particles originated from the Saharan region and approached Greece after passing over the Mediterranean Sea. Trajectory analysis suggests that air masses may often experience interaction with maritime aerosol before reaching the Greater Athens Area. The maximum dust load was predicted to occur over Athens on 28, 29 March and 2 April (Fig. 1).

Figure 2 presents back-trajectories calculated by the HYSPLIT model (Draxler et al., 2009) for the air masses arriving over Athens at 1, 2 and 3.5 km height levels at 12:00 UTC (left figure) and 19:00 UTC (right figure) on 2 April. The trajectories suggest that the air masses originated a week earlier from central, western and eastern Sahara (sometimes within the planetary boundary layer). Subsequently, they traversed over the central Mediterranean region and moved anti-cyclonically over Greece. More precisely, the air masses ending at 2 km height at 12:00 UTC were enriched with dust particles near the source passing at about 800 m a.s.l. (about 150 h before their arrival in Greece), while those ending at 3.5 km nearly touched the surface, thus they should contain much higher dust loads (Fig. 2, left). On the other hand, the air masses ending

## Optical-microphysical properties of Saharan dust aerosols

A. Papayannis et al.

Title Page

Abstract

Introduction

Conclusions

References

Tables

Figures



Back

Close

Full Screen / Esc

Printer-friendly Version

Interactive Discussion

at 3.5 km at 19:00 UTC were enriched twice with dust particles passing over the Sahara (about 150 and 30 h, before) (Fig. 2, right).

Aerosol backscatter and Raman measurements at 355, 532 and 1064 nm were performed by the NTUA Raman lidar system over Athens only under cloud-free conditions in the studied period. Thus, we will focus on aerosol profiles obtained on 2 April 2009. Figure 3 shows the time-height cross section of the range-corrected backscatter lidar signal (in arbitrary units: AU) obtained at 1064 nm from 13:42 to 20:49 UTC from 300 up to 6000 m a.s.l., after the cloud dissipation. According to the lidar measurements, the entire lower troposphere (from ground up to 3500–4000 m height) is very rich in aerosol particles. More specifically, two thin and distinct aerosol layers are shown, evolving during the period of measurements. The first layer was located around 2000 m, while the second one was found between 3200–3700 m. Indeed, the BSC-DREAM8b model indicates the transfer of Saharan dust particles over Athens (Fig. 1). These particles are mostly confined between 2 and 4 km height (Fig. 4) and have very high forecasted dust concentrations of the order of  $400 \mu\text{g m}^{-3}$  at 3 km. These dust heights are also in full accordance with the output of the HYSPLIT model indicating the arrival of dust-rich air masses over Athens originating from the Saharan desert, then passing over Algeria and Tunisia (Fig. 2).

Both aerosol layers detected by lidar slightly descended in height and became more diluted during the afternoon hours, although always present around 2000 m and 3200–3700 m. The Planetary Boundary Layer (PBL) height during daytime reached heights of about 1400 m around 14:00 UTC, while during the afternoon hours it descended down to 500 m a.s.l. around midnight, in full accordance with the closest radiosonde profile data (not shown here). The highest values of the range-corrected backscatter lidar signal within the PBL (shown by the red colour) indicate the possibility of dust presence also near ground, mixed with locally produced aerosols (e.g. by anthropogenic sources).

The mass concentration of  $\text{PM}_{10}$  particles measured in situ at 14 m above ground level, from 27 March to 2 April 2009, showed that during this dust event when the

## Optical- microphysical properties of Saharan dust aerosols

A. Papayannis et al.

Title Page

Abstract

Introduction

Conclusions

References

Tables

Figures



Back

Close

Full Screen / Esc

Printer-friendly Version

Interactive Discussion



layers (from 1.9 up to 4 km height) at 355 nm ( $LR = 83 \pm 8$  sr,  $ABR = 1.1$ ,  $AER = 0.9$ ) and 532 nm ( $LR = 60 \pm 7$  sr) are consistent with the relevant observations ( $LR = 30\text{--}80$  sr at 355 nm) performed over Athens (Papayannis et al., 2005) and those reported by Müller et al. (2009a, b), Tesche et al. (2009) and Wandinger et al. (2010), performed in the Saharan desert during the SAMUM experiment ( $LR \sim 50\text{--}80$  sr and  $ABR \sim 0$  to 0.5,  $AER \sim -0.3$  to 1 at 355 nm and  $LR \sim 50\text{--}100$  sr and  $ABR \sim 0.25$  to 0.75 at 532 nm), as well as those performed over Europe in the frame of the EARLINET project (Papayannis et al., 2008) ( $LR \sim 30\text{--}80$  sr at 355 nm,  $ABR \sim -0.5$  to 3 and  $LR \sim 50\text{--}55$  sr at 532 nm). In our case, the corresponding AOD was 0.53 and 0.31 at 355 and 532 nm, respectively.

Figure 6 shows the temporal evolution of the CIMEL sun photometer AOD at eight wavelengths and the Ångström exponent ( $\alpha$ ) over Athens for the period 27 March to 3 April 2009. The Ångström exponent ( $\alpha$ ) is derived according to the Ångström power law, using the 440, 670 and 870 nm channels (e.g. Eck et al., 1999; Holben et al., 2001). From the almucantar sky radiance measurements (see also <http://aeronet.gsfc.nasa.gov>) at the four highest wavelengths an inversion algorithm (AERONET version 2), as described by Dubovik et al. (2002, 2006), retrieves a large set of optical and microphysical aerosol parameters. In Fig. 6, the MODIS AODs at 550 nm are additionally presented (white squares) along with the BSC-DREAM8b dust AODs at 550 nm (upper panel). CIMEL data between 29 March and 1 April are lacking owing to excessive cloud cover over the city of Athens.

Moreover, the MODIS data for the wider area of Athens ( $10 \times 10$  km over the station) on 29 March, showed that the evolution of the event was well captured by the BSC-DREAM8b model. The BSC-DREAM8b data incorporated in Fig. 6, as AOD values, showed the quick arrival of the desert plume over the Athens station on 29 March, and then on 2 April. The highest CIMEL AOD was registered on 2 April with a value of 0.7 (440 nm). The desert dust plume was also visible on 3 April, while the following days (from 4 April) showed a clear weakening of the event as the desert plume quickly moved away, as shown by the AOD, which dropped back to background levels. The temporal evolution of the Ångström exponent (440–870 nm) for the same time period

## Optical- microphysical properties of Saharan dust aerosols

A. Papayannis et al.

Title Page

Abstract

Introduction

Conclusions

References

Tables

Figures

◀

▶

◀

▶

Back

Close

Full Screen / Esc

Printer-friendly Version

Interactive Discussion



is also shown in the lower panel, showing low values (from 0.4 to 1.0) for 2 and 3 April, in inverse correspondence with the high AOD for desert aerosols. One of the characteristics of the desert dust episodes in our area (Balis et al., 2004) is the high variability shown by both parameters during each day.

As can be seen in Fig. 6, on 2 April between 10:00 and 14:00 UTC, we observed high AODs due to strong dust layers which were advected to the observation location (as shown in lidar data). For the same day, the mean daily volume aerosol size distribution (not shown) exhibited two modes, but the relative importance of the modes depends on the prevailing aerosol type: an accumulation or fine mode with particle radius below 0.6  $\mu\text{m}$ , and a coarse mode with particle radius between 0.6 and 15  $\mu\text{m}$ . In this case, we expect a predominant coarse mode during desert dust conditions. The mode radii and volume concentrations were analyzed in order to characterize the aerosol dust evolution. The evolution of the desert dust is clear in the coarse mode fraction.

Table 1 presents the percent contribution of dust and sulfates to  $\text{PM}_{10}$ . The detailed calculations have already been presented in Remoundaki et al. (2011). From this Table, it can be seen that dust contribution was at the level of 15 % before the arrival of the Saharan dust and increased significantly during the dust event reaching 65 % on March 31 and 79 % on 1 April, respectively. Sulfates contribution ( $\text{SO}_4^{2-}$ ) was in expected levels and presented a maximum on 29 March where southerlies, (responsible for long-range transport of particles of crustal origin) were simultaneously present with west winds charged with aerosol particles from local urban and industrial emission sources (e.g. oil refineries of Aspropyrgos located in the WNW-NW sector) (Remoundaki et al., 2011). Finally, both dust and sulfates represent significant fraction of  $\text{PM}_{10}$  explaining in some cases more than 50 % of the  $\text{PM}_{10}$  mass.

The EDX analysis of all particles sampled (Remoundaki et al., 2011) during the reported period (27 March to 3 April 2009), revealed that aluminosilicates (clays) were predominant. The presence of illite was obvious in many cases, quartz particles were rare and very difficult to be detected. Dust particles were very rich in calcium which is distributed between calcite, dolomite and sulphates and Ca-Si particles (e.g.

## Optical- microphysical properties of Saharan dust aerosols

A. Papayannis et al.

Title Page

Abstract

Introduction

Conclusions

References

Tables

Figures

⏪

⏩

◀

▶

Back

Close

Full Screen / Esc

Printer-friendly Version

Interactive Discussion

smectites). Iron oxides were often detected. These results are in very good agreement and confirm those reported on the elemental composition of the dust and the origins of the air masses which first started from the Western Sahara and over passed northern Algeria on their way to Greece. These findings are also in very good agreement with literature on the Saharan particles characterization and their relationship to their origins (Coude-Gaussen G. et al., 1987; Avila et al., 1997; Blanco et al., 2003; Coz et al., 2009).

Using the aerosol backscatter profiles at 355, 532 and 1064 nm and the corresponding aerosol extinction profiles at 355 and 532 nm, we calculated the aerosol microphysical properties with the retrieval code for spheroid particles (Veselovskii et al., 2010) using the lidar data of 2 April. As mentioned previously, the retrieval algorithm represents the aerosol as a mixture of spheres and spheroids. However, without knowledge of the particle depolarization ratio (which provides a measure of the particle non-sphericity), the spheroid volume ratio (SVR) is underestimated, which leads to the underestimation of the real part of refractive index (Veselovskii et al., 2010). Thus, it is more accurate to suggest that the majority of the particle volume in the considered height range is related to non spherical particles. This assumption is justified by the HYSPLIT trajectories, which suggest that most of the particles in the coarse mode is associated with dust. The finer mode particles (and a fraction of the coarse dust) are expected to mix with anthropogenic pollution and sea salt; this, together with aerosol water will undoubtedly make particles more spherical.

We selected to retrieve the aerosol properties at four different layers for the period between 17:40–20:40 UT: layer 1 (1910–2070 m), layer 2 (2284–2850), layer 3 (2960–3100 m) and layer 4 (3140–3420 km). The retrieved particle volume size distributions  $dV/d\ln r$  for the four considered layers is shown in Fig. 7a. Moreover, the integral particle parameters, such as volume ( $V$ ), surface ( $S$ ), number ( $N$ ) densities, effective radius ( $r_{\text{eff}}$ ) and real ( $m_{\text{R}}$ ) and imaginary ( $m_{\text{i}}$ ) part of refractive index are summarized in Table 2. From the particle size distribution (PSD) analysis, shown in Fig. 7a we can conclude that the fine mode of the PSD is centered at 0.13  $\mu\text{m}$ , while the coarse

## Optical- microphysical properties of Saharan dust aerosols

A. Papayannis et al.

Title Page

Abstract

Introduction

Conclusions

References

Tables

Figures

⏪

⏩

◀

▶

Back

Close

Full Screen / Esc

Printer-friendly Version

Interactive Discussion

**Optical-  
microphysical  
properties of Saharan  
dust aerosols**

A. Papayannis et al.

Title Page

Abstract

Introduction

Conclusions

References

Tables

Figures

⏪

⏩

◀

▶

Back

Close

Full Screen / Esc

Printer-friendly Version

Interactive Discussion



mode is centered near 1 and 2  $\mu\text{m}$ . More specifically, at lower heights (layer 1) the fine mode is prevailing, but at higher altitudes the contribution of the coarse mode becomes more important. The fine mode containing the small particles determines the integral particle number density. In our case, the fine mode particles decrease, thus resulting in  $N$  decreasing from 1700  $\text{cm}^{-3}$  in the layer 1 to 700–800  $\text{cm}^{-3}$  in layers 3 and 4. On the other hand, the effective radius rises from 0.22  $\mu\text{m}$  to around 0.32  $\mu\text{m}$  between layer 1 and layers 3 and 4. In fact, the in situ aerosol sampling revealed that near the end of the Saharan dust event on 2 April, the dominant size of the particles diameter was smaller than 2  $\mu\text{m}$  (Remoundaki et al., 2011), which is consistent with the retrieved aerosol volume size distribution (Fig. 7a).

In Fig. 7b we show the aerosol size distribution (total column) measured by the CIMEL sun photometer for different hours (from 05:55:42 UTC to 13:30:45 UTC), where two main aerosol classes are found: those of fine (around 0.15  $\mu\text{m}$  radius) and those of coarse particles (around 1–2  $\mu\text{m}$  radius). Furthermore, if we divide the integrated CIMEL data (at 13:30:45 UTC) by the height of 4 km (where most of the dust are confined) we obtain maxima of the  $dV(r)/d\ln(r)$  of the order of 9 and 15  $\mu\text{m}^3 \text{cm}^{-3}$  for the fine and coarse mode, respectively. These maximum values are quite close to the maximum size distribution values (Fig. 7a) retrieved from the lidar data (5.5–12.5 and 7.5–10  $\mu\text{m}^3 \text{cm}^{-3}$ , respectively). Moreover, both Fig. 7a and b show comparable size distributions having radius centered around 0.15  $\mu\text{m}$  (fine mode) and 1 to 2  $\mu\text{m}$ , respectively. Although there is some difference, especially in the coarse (around 1  $\mu\text{m}$  radius) particles, temporal variability and non concurrent measurements between the retrievals could account for it.

Moreover, the retrieved real part of the refractive index is of the order of 1.47 in the layers 1 and 2, indicating mixing of dust with urban-like sulphate and organic carbon aerosols (Sokolik et al., 1993; Ebert et al., 2004; Raut and Chazette, 2008; McConnell et al., 2010), while in the layers 3 and 4 it increases up to 1.52, indicating the even stronger mixing of dust with urban-like sulphate and organic carbon aerosols over Athens (Ebert et al., 2002; Petzold et al., 2009). The imaginary part of refractive index

in all layers is  $m_1 = 0.007 \pm 0.0035$ , indicating non-urban influenced absorbing particles (Patterson et al., 1977; Sokolik et al., 1993; Sokolik and Toon, 1999; Ebert et al, 2004; Müller et al., 2009; Kandler et al., 2009).

It is interesting to note that the latest available Cimel data for 2 April, obtained at 13:30 UTC over Athens (not shown here), gave a columnar refractive index of the order of 1.53–1.55 (real part), while the imaginary part was ranging from 0.009i to 0.015i. These values represent column values which are obtained during the Saharan dust event several hours before the lidar sampling; they are typical of mixtures of silicate particles with sea salt (Ebert et al., 2002). Moreover, the retrieved mean columnar value of the effective radius was 0.21  $\mu\text{m}$  (at 13:30:45 UTC), which compares very well with the retrieved value (0.22  $\mu\text{m}$ ), from the lidar data at the dust layer 1 (between 17:40–20:40 UTC), but less with those retrieved from layers 2–4 (2.28–3.42 km), as shown in Table 2. Indeed, layers 2 to 4 (17:40 to 20:40 UTC) are related to the strong dust layer which appeared around 3.5 km (from 13:42 to 16:00 UTC) (see Fig. 3), therefore, they could be probably associated to bigger dust particles.

The final data set of the aerosol optical and microphysical properties along with the water vapor profiles were incorporated into the ISORROPIA II model (Fountoukis and Nenes, 2007) to infer the chemical parameters of the aerosols (e.g. dry chemical composition) that are consistent with the retrieved refractive index values (Table 2). For the aerosols located at layer 1, we derived a chemical composition of about 50–60 % sulfate, 15–25 % organic carbon (OC) and 15–35 % mineral dust is required for this. At the second layer, the model showed less concentration of sulfates and a slide increase of OC in comparison with the first one. Specifically, the retrieved chemical composition was of the order of 32–52 % for sulfates, 28–36 % for the OC and 12–40 % mineral dust. For the aerosols located at layer 3 we derived a chemical composition of about 18–38 % sulfate, 52–62 % OC and 0–30 % mineral dust. For the aerosols located at layer 4 a chemical composition of about 16–36 % sulfate, 54–64 % OC and 0–30 % mineral dust was estimated by the model. At the two upper layers the retrievals showed more concentration of OC which is correlating well with the high values of the refractive

## Optical- microphysical properties of Saharan dust aerosols

A. Papayannis et al.

[Title Page](#)[Abstract](#)[Introduction](#)[Conclusions](#)[References](#)[Tables](#)[Figures](#)[⏪](#)[⏩](#)[◀](#)[▶](#)[Back](#)[Close](#)[Full Screen / Esc](#)[Printer-friendly Version](#)[Interactive Discussion](#)

index (of the order of 1.52) and reflects the tendency of organic carbon to partition to the aerosols phase, under the cooler conditions at higher altitudes (Seinfeld and Pandis, 2008).

These findings, which indeed indicate mixing of mineral dust aerosols with sulfate and OC ones (typical from urban air pollution sources), are in accordance with the lidar data presented in Fig. 3, where the dust layered aerosols around 2000–3500 m (between 17:40–20:40 UT) are diluted over the PBL, through mixing with locally produced ones. Table 2 summarizes the optical, microphysical and chemical properties of aerosols retrieved at the four specific layers (1st to 4th layer), as well as the RH (%) at each layer for 2 April 2009. Regarding the percentage of mineral dust (34.5%) to PM<sub>10</sub> shown in Table 1, we see that the findings from the chemical analysis are in the upper limit values of those derived by the ISORROPIA II model for the lower atmospheric layers (1st and 2nd layers, located from 1.9 to 2.85 km a.s.l.). Given that OC is not measured, 34.5% is in reality the upper limit of dust concentration.

On the other hand, the percentage of SO<sub>4</sub><sup>2-</sup> contribution to PM<sub>10</sub> near ground (see Table 1) was much lower than the ones derived by the ISORROPIA II model for the lower atmospheric layers, but it agreed quite well with the lower limit values of those derived by the ISORROPIA II model for the upper atmospheric layers (3rd and 4th layers, located from 2.9 to 3.42 km a.s.l.). Given that the filter integrates over a larger period than the lidar (Remoundaki et al., 2011), the average chemical composition differs from the retrieval: furthermore, changes in acidity (due to uptake of ammonium) affect the mass associated with the sulfate ion by 40% (Seinfeld and Pandis, 2008).

## 4 Conclusions

In this manuscript, we attempted to combine experimental data (multi-wavelength Raman data (3 aerosol backscatter and 2 extinction profiles) and in situ measurements to chemically characterize the aerosol sampled) and models (microphysical inversion and thermodynamic ones), to infer the particle optical and microphysical properties as well as their chemical composition.

## Optical- microphysical properties of Saharan dust aerosols

A. Papayannis et al.

Title Page

Abstract

Introduction

Conclusions

References

Tables

Figures

⏪

⏩

◀

▶

Back

Close

Full Screen / Esc

Printer-friendly Version

Interactive Discussion



**Optical-  
microphysical  
properties of Saharan  
dust aerosols**

A. Papayannis et al.

Title Page

Abstract

Introduction

Conclusions

References

Tables

Figures

⏪

⏩

◀

▶

Back

Close

Full Screen / Esc

Printer-friendly Version

Interactive Discussion



During a strong Saharan dust event occurred over Athens (27 March to 3 April 2009), selected measurements were performed to observe the optical properties of the dust particles in the lower troposphere. A hybrid regularization technique was used to derive the mean microphysical properties of the dust particles, while the thermodynamic model ISORROPIA II was used to infer the aerosol chemical properties at four selected dust layers between 2.9 and 3.4 km. AOD values, derived from the CIMEL photometer, ranged from 0.53 (355 nm) to 0.31 (532 nm), while the LR values retrieved from the Raman lidar ranged from 75–100 sr (355 nm) and 50–70 sr (532 nm). Relative humidity of the order of 60–80 % and AE values related to backscatter of about 0.85–1.25 were observed inside the dust layers. The higher value of  $\alpha$  (1.25) observed at the lower atmospheric layer, indicates a probable mixing of the dust particles with locally produced particles, while the higher dust layers seemed to be less affected by the locally produced aerosols, since their AE values remained much lower (0.85–0.94) indicating the dominance of the coarse particles. In between the four selected dust layers mean aerosol refractive indexes of  $1.49(\pm 0.05) + 0.007(\pm 0.0035)i$  and effective radii ranging from  $0.22 \pm 0.06$  to  $0.33 \pm 0.1 \mu\text{m}$  were retrieved. The inferred chemical properties showed a 12–40 % of dust content, a sulphate composition of 16–60 %, and organic carbon content (OC) lower than 15–64 %. Indeed, the first two layers seemed to be more affected by the locally produced particles (higher sulphate and less dust contents), while the higher layers were less affected (lower sulphate and higher dust maxima contents). In situ airborne aerosol sampling together with multi-wavelength Raman lidar measurements should be performed to further evaluate the procedure proposed in this study.

*Acknowledgements.* The financial support for EARLINET (EARLINET-ASOS) by the European Commission under grant RICA-025991 and the European Space Agency (ESA-AO/1-5502/07/NL/HE) are gratefully acknowledged. The forecast of the dust transport model BSC-DREAM8b was provided by the Barcelona Supercomputing Center. Air masses back trajectories were produced with the Hybrid Single-Particle Lagrangian Integrated Trajectory model (NOAA). The authors gratefully acknowledge the NOAA Air Resources Laboratory (ARL) for the provision of the HYSPLIT transport and dispersion model. AN acknowledges support from

NASA-ACMAP. This research has been co-financed by the European Union (European Social Fund – ESF) and Greek national funds through the Operational Program “Education and Lifelong Learning” of the National Strategic Reference Framework (NSRF) – Research Funding Program: Heracleitus II. Investing in knowledge society through the European Social Fund.  
5 REM acknowledges the funding of the “Greek State Scholarship Foundation: IKY”. PK acknowledges the ESA financial support under ESTEC contract 21487/08/NL/HE.

## References

- Adams, P. J. and Seinfeld, J. H.: Predicting global aerosol size distributions in general circulation models, *J. Geophys. Res.*, 104, 13791–13823, doi:10.1029/2001JD001010, 2002.
- 10 Andreae, M. O.: Climatic effects of changing atmospheric aerosol levels, in: *World Survey of Climatology*, vol. 16, *Future Climate of the World*, edited by: Henderson-Sellers, A., 341–392, Elsevier, Amsterdam, 1995.
- Annesi-Maesano, I., Forastiere, F., Kunzli, N., and Brunekref B.: Particulate matter, science and EU policy, *Eur. Respir. J.*, 29, 428–431, doi:10.1183/09031936.00129506, 2007.
- 15 Ansmann A., Riebesell, M., Wandinger, U., Weitkamp, C., Voss, C., Lahmann, W. and Michaelis, W.: Combined Raman Elastic-Backscatter lidar for vertical profiling of moisture, aerosol extinction, backscatter, and lidar ratio, *Appl. Phys. B*, 55, 18–28, 1992.
- Ansmann, A., Bösenberg, J., Chaikovskiy, A., Comeron, A., Eckhardt, S., Eixmann, R., Freudenthaler, V., Ginoux, P., Komguem, L., Linne, H., Lopez Marquez, M. A., Matthias, V., Mattis, I., Mitev, V., Müller, D., Music, S., Nickovic, S., Pelon, J., Sauvage, L., Sobolewsky, P., Srivastava, M. K., Stohl, A., Torres, O., Vaughan, G., Wandinger, U., and Wiegner, M.: Long-range transport of Saharan dust to northern Europe: The 11–16 October 2001 outbreak observed with EARLINET, *J. Geophys. Res.*, 108(D24), 4783, doi:10.1029/2003JD003757, 2003.
- 20 Ansmann, A., Mattis, I., Müller, D., Wandinger, U., Radlach, M., and Althausen, D.: Ice formation in Saharan dust over central Europe observed with temperature/humidity/aerosol Raman lidar, *J. Geophys. Res.*, 110, D18S12, doi:10.1029/2004JD005000, 2005.
- Avila, A., Queralt-Mitjans, I., and Alarcon, M.: Mineralogical composition of African dust delivered by red rains over northeastern Spain, *J. Geophys. Res.*, 108, 21977–21996, 1997.
- 25 Balis, D. S., Amiridis, V., Nickovic, S., Papayannis, A., and Zerefos, C.: Optical properties of

## Optical- microphysical properties of Saharan dust aerosols

A. Papayannis et al.

Title Page

Abstract

Introduction

Conclusions

References

Tables

Figures

⏪

⏩

◀

▶

Back

Close

Full Screen / Esc

Printer-friendly Version

Interactive Discussion



## Optical- microphysical properties of Saharan dust aerosols

A. Papayannis et al.

[Title Page](#)
[Abstract](#)
[Introduction](#)
[Conclusions](#)
[References](#)
[Tables](#)
[Figures](#)




[Back](#)
[Close](#)
[Full Screen / Esc](#)
[Printer-friendly Version](#)
[Interactive Discussion](#)


Saharan dust layers as detected by a Raman lidar at Thessaloniki, Greece, *Geophys. Res. Lett.*, 31, L13104, doi:10.1029/2004GL019881, 2004.

Balkanski, Y., Schulz, M., Claquin, T., and Guibert, S.: Reevaluation of Mineral aerosol radiative forcings suggests a better agreement with satellite and AERONET data, *Atmos. Chem. Phys.*, 7, 81–95, doi:10.5194/acp-7-81-2007, 2007.

Berthier, S., Chazette, P., Couvert, P., Pelon, J., Dulac, F., Thieuleux, F., Moulin, C., and Pain, T.: Desert dust aerosol columnar properties over ocean and continental Africa from Lidar in-Space Technology Experiment (LITE) and Meteosat synergy, *J. Geophys. Res.*, 111, D21202, doi:10.1029/2005JD006999, 2006.

Blanco, A., Dee Tomasi, F., Filippo, E., Manno, D., Perrone, M. R., Serra, A., Tafuro, A. M., and Tepore, A.: Characterization of African dust over southern Italy, *Atmos. Chem. Phys.*, 3, 2147–2159, doi:10.5194/acp-3-2147-2003, 2003.

Chan L. Y., Lau, W. L., Lee, S. C., and Chan, C. Y.: Commuter exposure to particulate matter in public transportation modes in Hong Kong, *Atmos. Environ.*, 36, 3363–3373, 2002.

Chu, D. A., Kaufman, Y. J., Zibordi, G., Chern, J. D., Mao, J., Li, C., and Holben, B. N.: Global monitoring of air pollution over land from the Earth Observing System-Terra Moderate Resolution Imaging Spectroradiometer (MODIS), *J. Geophys. Res.*, 108(D21), 4661, doi:10.1029/2002JD003179, 2003.

Coude-Gaussen, G., Rognon, P., Bergametti, G., Gomez, L., Strauss, B., Gros, J. M., and Le Costumer, N.: Saharan dust over Fuerteventura island (Canaries): chemical and mineralogical characteristics, air mass trajectories, and probable sources, *J. Geophys. Res.*, 92, 9753–9771, 1987.

Coz, E., Gomez-Moreno, F. J., Pujadas, M., Casuccio, G. S., Lersh, T. L., and Artinao, B.: Individual particle characteristics of North African dust under different long-transport scenarios, *Atmos. Environ.*, 43, 1850–1863, 2009.

Draxler, R. R., Stunder, B., Rolph, G., and Talyor, A.: *Hysplit 4 User's Guide*, NOAA Air Resources Laboratory, Silver Spring, MD, USA, 2009.

Dubovik, O., Sinyuk, A., Lapyonok, T., Holben, B. N., Mishenko, M., Yang, P., Eck, T. F., Volten, H., Munoz, O., Veihelmann, B., van der Zande, W. J., Leon, J.-F., Sorokin, M., and Slutsker, I.: Application of spheroid models to account for aerosol particle nonsphericity in remote sensing of desert dust, *J. Geophys. Res.*, 111, D11208, doi:10.1029/2005JD006619, 2006.

Ebert, M., Weinbruch, S., Rausch, A., Gorzawski, G., Hoffmann, P., Wex, H., and Helas, G.: Complex refractive index of aerosols during LACE 98 as derived from the analysis of individ-

## Optical-microphysical properties of Saharan dust aerosols

A. Papayannis et al.

Title Page

Abstract

Introduction

Conclusions

References

Tables

Figures

⏪

⏩

◀

▶

Back

Close

Full Screen / Esc

Printer-friendly Version

Interactive Discussion



ual particles, *J. Geophys. Res.*, 107(D21), 8121, doi:10.1029/2000JD000195, 2002.

Ebert, M., Weinbruch, S., Hoffmann, P., and Ortner, H. M.: The chemical composition and complex refractive index of rural and urban influenced aerosols determined by individual particle analysis, *Atmos. Environ.*, 38, 6531–6545, 2004.

5 EN12341, Air quality. Determination of the PM<sub>10</sub> fraction of suspended particulate matter. Reference method and field test procedure to demonstrate reference equivalence of measurement methods, ISBN: 0 580 32078 2, 18 pp., 1999.

Feingold, G., Yang, S., Hardesty, R. M., and Cotton, W. R.: Feasibility of retrieving Cloud Condensation Nucleus properties from Doppler cloud radar, microwave radiometer, and lidar, *J. Atmos. Oceanic Technol.*, 15, 1188–1195, 1998.

10 Feingold, G. and Morley, B.: Aerosol hygroscopic properties as measured by lidar and comparison with in situ measurements, *J. Geophys. Res.*, 108(D11), 4327, doi:10.1029/2002JD002842, 2003.

15 Forster, P., Ramaswamy, V., Artaxo, P., Bernsten, T., Betts, R., Fahey, D. W., Haywood, J., Lean, J., Lowe, D. C., Myhre, G., Nganga, J., Prinn, R., Raga, G., Schulz, M., and Van Dorland, R.: Changes in Atmospheric Constituents and in Radiative Forcing, in: *Climate Change 2007: The Physical Science Basis. Contribution of Working Group I to the Fourth Assessment Report of the Intergovernmental Panel on Climate Change*, edited by: Solomon, S., Qin, D., Manning, M., Chen, Z., Marquis, M., Averyt, K. B., Tignor, M., and Miller, H. L., Cambridge University Press, Cambridge, UK, 129–234, 2007.

20 Fountoukis C., and Nenes, A.: ISORROPIA II: a computationally efficient thermodynamic equilibrium model for K<sup>+</sup>–Ca<sup>2+</sup>–Mg<sup>2+</sup>–NH<sup>+</sup><sub>4</sub>–Na<sup>+</sup>–SO<sup>2-</sup><sub>4</sub>–NO<sup>-3</sup>–Cl<sup>-</sup>–H<sub>2</sub>O aerosols, *Atmos. Chem. Phys.*, 7, 4639–4659, doi:10.5194/acp-7-4639-2007, 2007.

25 Fountoukis, C., Nenes, A., Sullivan, A., Weber, R., Van Reken, T., Fischer, M., Matías, E., Moya, M., Farmer, D., and Cohen, R. C.: Thermodynamic characterization of Mexico City aerosol during MILAGRO 2006, *Atmos. Chem. Phys.*, 9, 2141–2156, doi:10.5194/acp-9-2141-2009, 2009.

Ganor, E., Osetinsky, I., Stupp, A., and Alpert, P.: Increasing trend of African dust, over 49 years, in the eastern Mediterranean, *J. Geophys. Res.*, 115, D07201, doi:10.1029/2009JD012500, 2010.

30 Ghan, S. and Collins, D. R.: Use of in situ data to test a Raman lidar–based cloud condensation nuclei remote sensing method, *J. Atmos. Ocean. Tech.*, 21, 387–394, 2004.

Haustein, K., Pérez, C., Baldasano, J. M., Müller, D., Tesche, M., Schladitz, A., Esselborn, M.,

## Optical- microphysical properties of Saharan dust aerosols

A. Papayannis et al.

[Title Page](#)
[Abstract](#)
[Introduction](#)
[Conclusions](#)
[References](#)
[Tables](#)
[Figures](#)




[Back](#)
[Close](#)
[Full Screen / Esc](#)
[Printer-friendly Version](#)
[Interactive Discussion](#)


- Weinzier, B., Kandler, K., and von Hoyningen-Huene, W.: Regional dust model performance during SAMUM 2006, *Geophys. Res. Lett.*, 36, L03812, doi:10.1029/2008GL036463, 2009.
- Helmert, J., Heinold, B., Tegen, I., Hellmuth, O., and Wendisch, M.: On the direct and semidirect effects of Saharan dust over Europe: A modeling study, *J. Geophys. Res.*, 112, D13208, doi:10.1029/2006JD007444, 2007.
- Heinold, B., Helmert, J., Hellmuth, O., Wolke, R., Ansmann, A., Marticorena, B., Laurent, B., and Tegen, I.: Regional modeling of Saharan dust events using LM-MUSCAT: Model description and case studies, *J. Geophys. Res.*, 112, D11204, doi:10.1029/2006JD007443, 2007.
- Holben, B. N., Eck, T. F., Slutsker, I., Tanré, D., Buis, J. P., Setzer, A., Vermote, E., Reagan, J. A., Kaufman, Y. J., Nakajima, T., Lavenu, F., Jankowiak, I., and Smirnov, A.: AERONET-A federated instrument network and data archive for aerosol characterization, *Remote Sens. Environ.*, 66(1), 1–16, doi:10.1016/S0034-4257(98)00031-5, 1998.
- Jiménez-Guerrero, P., Pérez, C., Jobra, O., and Baldasano, J.: Contribution of Saharan dust in an ingrated air quality system and its on-line assessment, *Geophys. Res. Lett.*, 35, L03814, doi:10.1029/2007GL031580, 2008.
- Kandler, K., Schütz, L., Deutscher, C., Hofmann, H., Jäckel, S., Knippertz, P., Lieke, K., Maßling, A., Schladitz, A., Weinzierl, B., Zorn, S., Ebert, M., Jaenicke, R., Petzold, A., and Weinbruch, S.: Size distribution, mass concentration, chemical and mineralogical composition, and derived optical parameters of the boundary layer aerosol at Tinfou, Morocco, during SAMUM 2006, *Tellus*, 61B, 32–50, 2009.
- Karydis, V. A., Tsimpidi, A. P., Fountoukis, C., Nenes, A., Zavala, M., Lei, W., Molina, L. T., and Pandis, S. N.: Simulating the fine and coarse inorganic particulate matter concentrations in a polluted megacity, *Atmos. Environ.*, 44, 608–620, 2010.
- Kaufman, Y. and Tanré, D.: Algorithms for remote sensing of tropospheric aerosol from MODIS. NASA MODIS Algorithm Theoretical Basis Document, Goddard Space Flight Center, 85 pp., 1998.
- Kinne, S., Schulz, M., Textor, C., Guibert, S., Balkanski, Y., Bauer, S. E., Berntsen, T., Berglen, T. F., Boucher, O., Chin, M., Collins, W., Dentener, F., Diehl, T., Easter, R., Feichter, J., Fillmore, D., Ghan, S., Ginoux, P., Gong, S., Grini, A., Hendricks, J., Herzog, M., Horowitz, L., Isaksen, I., Iversen, T., Kirkevåg, A., Kloster, S., Koch, D., Kristjansson, J. E., Krol, M., Lauer, A., Lamarque, J. F., Lesins, G., Liu, X., Lohmann, U., Montanaro, V., Myhre, G., Penner, J., Pitari, G., Reddy, S., Seland, O., Stier, P., Takemura, T., and Tie, X.: An AeroCom initial

## Optical- microphysical properties of Saharan dust aerosols

A. Papayannis et al.

[Title Page](#)
[Abstract](#)
[Introduction](#)
[Conclusions](#)
[References](#)
[Tables](#)
[Figures](#)




[Back](#)
[Close](#)
[Full Screen / Esc](#)
[Printer-friendly Version](#)
[Interactive Discussion](#)


assessment – optical properties in aerosol component modules of global models, *Atmos. Chem. Phys.*, 6, 1815–1834, doi:10.5194/acp-6-1815-2006, 2006.

Klein, H., Nickovic, S., Haunold, W., Bundke, U., Nillius, B., Ebert, M., Weinbruch, S., Schuetz, L., Levin, Z., Barrie, L. A., and Bingemer, H.: Saharan dust and ice nuclei over Central Europe, *Atmos. Chem. Phys.*, 10, 10211–10221, doi:10.5194/acp-10-10211-2010, 2010.

Laurent, B., Marticorena, B., Bergametti, G., Léon, J. F., and Mahowald, N. M.: Modeling mineral dust emissions from the Sahara desert using new surface properties and soil database, *J. Geophys. Res.*, 113, D14218, doi:10.1029/2007JD009484, 2008.

Levin, Z. and Cotton, W.: *Aerosol Pollution Impact on Precipitation: A Scientific Review*, Springer, New York, 2009.

Levy, R. C., Remer, L. A., Mattoo, S., Vermote, E. F., and Kaufman, Y. J.: Second generation operational algorithm: Retrieval of aerosol properties over land from inversion of Moderate Resolution Imaging Spectrometer spectral reflectance, *J. Geophys. Res.*, 112, D13211, doi:10.1029/2006JD007811, 2007.

Levy, R. C., Remer, L. A., Kleidman, R. G., Mattoo, S., Ichoku, C., Kahn, R., and Eck, T. F.: Global evaluation of the Collection 5 MODIS dark-target aerosol products over land, *Atmos. Chem. Phys.*, 10, 10399–10420, doi:10.5194/acp-10-10399-2010, 2010.

Liu, Z., Winker, D., Omar, A., Vaughan, M., Treppe, C., Hu, Y., Powell, K., Sun, W., and Lin, B.: Effective lidar ratios of dense dust layers over North Africa derived from the CALIOP measurements, *J. Quantum Spectrosc. Ra.*, 112, 204–213, 2011.

Lohmann, U., Rotstajn, L., Storelmo, T., Jones, A., Menon, S., Quaas, J., Ekman, A. M. L., Koch, D., and Ruedy, R.: Total aerosol effect: radiative forcing or radiative flux perturbation?, *Atmos. Chem. Phys.*, 10, 3235–3246, doi:10.5194/acp-10-3235-2010, 2010.

Mahowald, N. M., Yoshioka, M., Collins, W. D., Conley, A. J., Fillmore, D. W., and Coleman, D. B.: Climate response and radiative forcing from mineral aerosols during the last glacial maximum, pre-industrial, current and doubled-carbon dioxide climates, *Geophys. Res. Lett.*, 33, L20705, doi:10.1029/2006gl026126, 2006.

Mamouri R.E., Papayannis, A., Tsaknakis, G., Amiridis, V., and Koukouli, M.: First water vapor measurements over Athens, Greece, obtained by a combined Raman-elastic backscatter lidar system, *Opt. Pura Aplic.*, 41, 109–116, 2008.

Mamouri, R. E., Amiridis, V., Papayannis, A., Giannakaki, E., Tsaknakis, G., and Balis, D. S.: Validation of CALIPSO space-borne-derived attenuated backscatter coefficient profiles using a ground-based lidar in Athens, Greece, *Atmos. Meas. Tech.*, 2, 513–522, doi:10.5194/amt-

## Optical- microphysical properties of Saharan dust aerosols

A. Papayannis et al.

[Title Page](#)
[Abstract](#)
[Introduction](#)
[Conclusions](#)
[References](#)
[Tables](#)
[Figures](#)




[Back](#)
[Close](#)
[Full Screen / Esc](#)
[Printer-friendly Version](#)
[Interactive Discussion](#)

2-513-2009, 2009.

Marticorena, B., Bergametti, G., Aumont, B., Callot, Y., N'Doumé, C., and Legrand, M.: Modelling the atmospheric dust cycle: 2. Simulation of Saharan sources, *J. Geophys. Res.*, 102, 4387–4404, doi:10.1029/96JD02964, 1997.

5 Mattis I., Müller, D., Ansmann, A., Wandinger, U., Preissler, J., Seifert, P., and Tesche, M.: Ten years of multiwavelength Raman lidar observations of free-tropospheric aerosol layers over central Europe: Geometrical properties and annual cycle, *J. Geophys. Res.*, 113, D20202, doi:10.1029/2007JD009636, 2008.

McConnell, C. L., Formenti, P., Highwood, E. J., and Harrison, M. A. J.: Using aircraft measurements to determine the refractive index of Saharan dust during the DODO Experiments, *Atmos. Chem. Phys.*, 10, 3081–3098, doi:10.5194/acp-10-3081-2010, 2010.

10 Merikallio, S., Lindqvist, H., Nousiainen, T., and Kahnert, M.: Modelling light scattering by mineral dust using spheroids: assessment of applicability, *Atmos. Chem. Phys.*, 11, 5347–5363, doi:10.5194/acp-11-5347-2011, 2011.

15 Metzger, S., Mihalopoulos, N., and Lelieveld, J.: Importance of mineral cations and organics in gas-aerosol partitioning of reactive nitrogen compounds: case study based on MINOS results, *Atmos. Chem. Phys.*, 6, 2549–2567, doi:10.5194/acp-6-2549-2006, 2006.

Min, Q.-L., Li, R., Lin, B., Joseph, E., Wang, S., Hu, Y., Morris, V., and Chang, F.: Evidence of mineral dust altering cloud microphysics and precipitation, *Atmos. Chem. Phys.*, 9, 3223–3231, doi:10.5194/acp-9-3223-2009, 2009.

20 Mishchenko, M. I., Travis, L. D., Kahn, R. A., and West, R. A.: Modeling phase functions for dustlike tropospheric aerosols using a mixture of randomly oriented polydisperse spheroids, *J. Geophys. Res.*, 102, 16831–16847, 1997.

Misra, A., Jayaraman, A., and Ganguly, D.: Validation of MODIS derived aerosol optical depth over Western India, *J. Geophys. Res.*, 113, D04203, doi:10.1029/2007JD009075, 2008.

25 Moya, M., Ansari, A. S., and Pandis, S. N.: Partitioning of nitrate and ammonium between the gas and particulate phases during the 1997 IMADA-AVER study in Mexico City, *Atmos. Environ.*, 35, 1791–1804, 2001.

Müller, D., Wandinger, U., and Ansmann, A.: Microphysical particle parameters from extinction and backscatter lidar data by inversion with regularization: theory, *Appl. Opt.*, 38, 2346–2357, 1999.

30 Müller, D., Mattis, I., Wandinger, U., Ansmann, A., Althausen, D., and Stohl, A.: Raman lidar observations of aged Siberian and Canadian forest-fire smoke in the free troposphere over

## Optical- microphysical properties of Saharan dust aerosols

A. Papayannis et al.

[Title Page](#)[Abstract](#)[Introduction](#)[Conclusions](#)[References](#)[Tables](#)[Figures](#)[⏪](#)[⏩](#)[◀](#)[▶](#)[Back](#)[Close](#)[Full Screen / Esc](#)[Printer-friendly Version](#)[Interactive Discussion](#)

Germany in 2003: microphysical particle characterization, *J. Geophys. Res.*, 110, D17201, doi:10.1029/2004JD005756, 2005.

Müller, D., Heinold, B., Tesche, M., Tegen, I., Althausen, D., Amiridis, V., Amodeo, A., Ansmann, A., Alados-Arboledas, L., Balis, D., Comeron, A., D'Amico, G., Gerasopoulos, E., Freudenthaler, V., Giannakaki, E., Heese, B., Iarlori, M., Mamouri, R. E., Mona, L., Papayannis, A., Pappalardo, G., Perrone, R.-M., Pisani, G., Rizi, V., Sicard, M., Spinelli, N., and Tafuro, A.: EARLINET Observations of the 14–22 May Long-Dust Transport Event During SAMUM 2006: Validation Results From Dust Transport Modelling”, *Tellus*, 61B, 325–339, 2009a.

Müller, T., Schladitz, A., Massling, A., Kaaden, A., Kandler, K., and Wiedensohler, A.: Spectral absorption coefficients and imaginary parts of refractive indices of Saharan dust during SAMUM-1, *Tellus*, 61B, 79–95, 2009b.

Müller, D., Weinzierl, B., Petzold, A., Kandler, K., Ansmann, A., Müller, T., Tesche, M., Freudenthaler, V., Esselborn, M., Heese, B., Althausen, D., Schladitz, A., Otto, S., and Knippertz, P.: Mineral dust observed with AERONET Sun photometer, Raman lidar, and in situ instruments during SAMUM 2006: Shape-independent particle properties, *J. Geophys. Res.*, 115, D07202, doi:10.1029/2009JD012520, 2010.

Nickovic, S., Kallos, G., Papadopoulos, A., and Kakaliagou, O.: A model for prediction of desert dust cycle in the atmosphere, *J. Geophys. Res.*, 106, 18113–18129, 2001.

Nowak, J. B., Huey, L. G., Russell, A. G., Tian, D., Neuman, J. A., Orsini, D., Sjostedt, S. J., Sullivan, A. P., Tanner, D. J., Weber, R. J., Nenes, A., Edgerton, E., and Fehsenfeld, F. C.: Analysis of urban gas phase ammonia measurements from the 2002 Atlanta Aerosol Nucleation and Real-Time Characterization Experiment (ANARChE), *J. Geophys. Res.*, 111, D17308, doi:10.1029/2006JD007113, 2006.

Pahlow, M., Müller, D., Tesche, M., Eichler, H., Feingold, G., Eberhard, W. L., and Cheng, Y.-F.: Retrieval of aerosol properties from combined multiwavelength lidar and sunphotometer measurements, *Appl. Opt.*, 45, 7429–7442, 2006.

Papadimas, C. D., Hatzianastassiou, N., Mihalopoulos, N., Kanakidou, M., Katsoulis, B. D., and Vardavas, I.: Assessment of the MODIS Collections C005 and C004 aerosol optical depth products over the Mediterranean basin, *Atmos. Chem. Phys.*, 9, 2987–2999, doi:10.5194/acp-9-2987-2009, 2009.

Papayannis, A., Balis, D., Amiridis, V., Chourdakis, G., Tsaknakis, G., Zerefos, C., Castanho, A. D. A., Nickovic, S., Kazadzis, S., and Grabowski, J.: Measurements of Saharan dust aerosols over the Eastern Mediterranean using elastic backscatter-Raman lidar, spectrophotometric

## Optical- microphysical properties of Saharan dust aerosols

A. Papayannis et al.

[Title Page](#)
[Abstract](#)
[Introduction](#)
[Conclusions](#)
[References](#)
[Tables](#)
[Figures](#)




[Back](#)
[Close](#)
[Full Screen / Esc](#)
[Printer-friendly Version](#)
[Interactive Discussion](#)


and satellite observations in the frame of the EARLINET project, *Atmos. Chem. Phys.*, 5, 2065–2079, doi:10.5194/acp-5-2065-2005, 2005.

Papayannis, A., Amiridis, V., Mona, L., Tsaknakis, G., Balis, D., Bösenberg, J., Chaikovski, A., De Tomasi, F., Grigorov, I., Mattis, I., Mitev, V., Müller, D., Nickovic, S., Perez, C., Pietruczuk, A., Pisani, G., Ravetta, F., Rizi, V., Sicard, M., Trickl, T., Wiegner, M., Gerd-  
ing, M., Mamouri, R.E., D'Amico, G., and Pappalardo, G.: Systematic lidar observations of  
Saharan dust over Europe in the frame of EARLINET (2000–2002), *J. Geophys. Res.*, 113,  
D10204, doi:10.1029/2007JD009028, 2008.

Patterson, E. M., Filette, D. A., and Stockton, B. H.: Complex index of refraction between 300  
and 700 nm for Saharan aerosols, *J. Geophys. Res.*, 82, 3153–3160, 1977.

Pérez, C., Nickovic, S., Baldasano, J. M., Sicard, M., Rocadenbosch, F., and Cachorro,  
V. E.: A long Saharan dust event over the western Mediterranean: Lidar, Sun pho-  
tometer observations, and regional dust modeling, *J. Geophys. Res.*, 111, D15214,  
doi:10.1029/2005JD006579, 2006a.

Pérez, C., Nickovic, S., Pejanovic, G., Baldasano, J. M., and Özsoy, E.: Interactive dust-  
radiation modeling: A step to improve weather forecasts, *J. Geophys. Res.*, 111, D16206,  
doi:10.1029/2005JD006717, 2006b.

Petzold, A., Rasp, K., Weinzierl, B., Esselborn, M., Hamburger, T., Dornbrack, Kandler, K.,  
Schutz, L., Knippertz, P., Fiebig, M., and Virkkula, A.: Saharan dust absorption and refrac-  
tive index from aircraft-based observations during SAMUM 2006, *Tellus B*, 61(1), 118–130,  
2009.

Prasad, A. K. and Singh, R. P.: Validation of MODIS Terra, AIRS, NCEP/DOE AMIP-  
II Reanalysis-2, and AERONET Sun photometer derived integrated precipitable water  
vapor using ground-based GPS receivers over India, *J. Geophys. Res.*, 114, D05107,  
doi:10.1029/2008JD011230, 2009.

Pringle, K. J., Tost, H., Message, S., Steil, B., Giannadaki, D., Nenes, A., Fountoukis, C.,  
Stier, P., Vignati, E., and Lelieveld, J.: Description and evaluation of GMXe: a new aerosol  
submodel for global simulations (v1), *Geosci. Model Dev.*, 3, 391–412, doi:10.5194/gmd-3-  
391-2010, 2010.

Pye, H. O. T., Liao, H., Wu, S., Mickley, L. J., Jacob, D. J., Henze D. K., and Seinfeld J. H.: Effect  
of changes in climate and emissions on future sulfate-nitrate-ammonium aerosol levels in the  
United States, *J. Geophys. Res.*, 114, D01205, doi:10.1029/2008JD010701, 2009.

Ramanathan, V., Crutzen, P. J., Kiehl, J. T., and Rosenfeld, D.: Aerosols, climate and the

## Optical- microphysical properties of Saharan dust aerosols

A. Papayannis et al.

[Title Page](#)
[Abstract](#)
[Introduction](#)
[Conclusions](#)
[References](#)
[Tables](#)
[Figures](#)




[Back](#)
[Close](#)
[Full Screen / Esc](#)
[Printer-friendly Version](#)
[Interactive Discussion](#)


hydrological cycle, *Science*, 294, 2119–2123, doi:10.1126/science.1064034, 2001.

Ramanathan, V. and Feng, Y.: Air pollution, greenhouse gases and climate change: Global and regional perspectives, *Atmos. Environ.*, 43, 37–50, 2009.

Raut, J.-C. and Chazette, P.: Vertical profiles of urban aerosol complex refractive index in the frame of ESQUIF airborne measurements, *Atmos. Chem. Phys.*, 8, 901–919, doi:10.5194/acp-8-901-2008, 2008.

Remer, L. A., Kaufman, Y. J., Tarré, D., Mattoo, S., Chu, D. A., Martins, J. V., Li, R.-R., Cichoku, C., Levy, R. C., Kleidman, R. G., Eck, T. F., Vermote, E., and Holben, B. N.: The MODIS Aerosol Algorithm, Products, and Validation, *J. Atmos. Sci.*, 62, 947–973, 2005.

Remoundaki, E., Bourliva, A., Kokkalis, Mamouri, R.E., P., Papayannis, A., Grigoratos, T., Samara, C., and Tsezos, M.: Composition of PM<sub>10</sub> during a Saharan dust transport event over Athens, Greece, *Sci. Total Environ.*, 409, 4361–4372, doi:10.1016/j.scitotenv.2011.06.026, 2011.

San Martini, F. M., Dunlea, E. J., Volkamer, R., Onasch, T. B., Jayne, J. T., Canagaratna, M. R., Worsnop, D. R., Kolb, C. E., Shorter, J. H., Herndon, S. C., Zahniser, M. S., Salcedo, D., Dzepina, K., Jimenez, J. L., Ortega, J. M., Johnson, K. S., McRae, G. J., Molina, L. T., and Molina, M. J.: Implementation of a Markov Chain Monte Carlo method to inorganic aerosol modeling of observations from the MCMA-2003 campaign – Part II: Model application to the CENICA, Pedregal and Santa Ana sites, *Atmos. Chem. Phys.*, 6, 4889–4904, doi:10.5194/acp-6-4889-2006, 2006.

Santese, M., De Tomasi, F., and Perrone, M. R.: Advection patterns and aerosol optical and microphysical properties by AERONET over south-east Italy in the central Mediterranean, *Atmos. Chem. Phys.*, 8, 1881–1896, doi:10.5194/acp-8-1881-2008, 2008.

Satheesh, S. K. and Moorthy, K. K.: Radiative effects of natural aerosols: A review, *Atmos. Environ.*, 39, 2089–2110, doi:10.1016/j.atmosenv.2004.12.029, 2005.

Sciare, J., Bardouki, H., Moulin, C., and Mihalopoulos, N.: Aerosol sources and their contribution to the chemical composition of aerosols in the Eastern Mediterranean Sea during summertime, *Atmos. Chem. Phys.*, 3, 291–302, doi:10.5194/acp-3-291-2003, 2003.

Seinfeld, J. H and S. Pandis, *Atmospheric Chemistry and Physics – From Air Pollution to Climate Change* (2nd Edition), John Wiley & Sons, 2006.

Shao, Y., Yang, Y., Wang, J., Song, Z., Leslie, L. M., Dong, C., Zhang, Z., Lin, Z., Kanai, Y., Yabuki, S., and Chun, Y.: Northeast Asian dust storms: Real-time numerical prediction and validation, *J. Geophys. Res.*, 108(D22), 4691, doi:10.1029/2003JD003667, 2003.

## Optical- microphysical properties of Saharan dust aerosols

A. Papayannis et al.

[Title Page](#)
[Abstract](#)
[Introduction](#)
[Conclusions](#)
[References](#)
[Tables](#)
[Figures](#)




[Back](#)
[Close](#)
[Full Screen / Esc](#)
[Printer-friendly Version](#)
[Interactive Discussion](#)

- Sokolik, I. N., Andronova, A., and Johnson, T. C.: Complex refractive index of atmospheric dust aerosols, *Atmos. Environ.*, 27A, 2495–2502, 1993.
- Sokolik, I. N. and Toon, O. B.: Incorporation of mineralogical composition into models of the radiative properties of mineral aerosol from UV to IR wavelengths, *J. Geophys. Res.*, 104, 9423–9444, 1999.
- Tanré, D., Kaufman, Y. J., Herman, M., and Mattoo, S.: Remote sensing of aerosol properties over oceans using the MODIS/ESO spectral radiances, *J. Geophys. Res.*, 102, 16971–16988, 1997.
- Terzi E., Argyropoulos G., Bougatioti, A., Mihalopoulos, N., Nikolaou, K., and Samara C.: Chemical composition and mass closure of ambient PM<sub>10</sub> at urban sites, *Atmos. Environ.*, 44, 2231–2239, 2010.
- Tesche, M., Ansmann, A., Müller, D., Althausen, D., Engelmann, R., Freudenthaler, V., and Groß, S.: Vertically resolved separation of dust and smoke over Cape Verde using multi-wavelength Raman and polarization lidars during Saharan Mineral Dust Experiment 2008, *J. Geophys. Res.*, 114, D13202, doi:10.1029/2009JD011862, 2009.
- Veselovskii, I., Kolgotin, A., Griaznov, V., Müller, D., Wandinger, U., and Whiteman, D. N.: Inversion with regularization for the retrieval of tropospheric aerosol parameters from multi-wavelength lidar sounding, *Appl. Opt.*, 41, 3685–3699, 2002.
- Veselovskii, I., Whiteman, D. N., Kolgotin, A., Andrews, E., and Korenskii, M.: Demonstration of aerosol property profiling by multi-wavelength lidar under varying relative humidity conditions, *J. Atmos. Ocean. Tech.*, 26, 1543–1557, 2009.
- Veselovskii, I., Dubovik, O., Kolgotin, A., Lapyonok, T., Di Girolamo, P., Summa, D., Whiteman, D. N., Mishchenko, M., and Tanré, D.: Application of randomly oriented spheroids for retrieval of dust particle parameters from multi-wavelength lidar measurements, *J. Geophys. Res.*, 115, D21203, doi:10.1029/2010JD014139, 2010.
- Wandinger, U., Tesche, M., Seifert, P., Ansmann, A., Müller, D., and Althausen, D.: Size matters: Influence of multiple scattering on CALIPSO light extinction profiling in desert dust, *Geophys. Res. Lett.*, 37, L10801, doi:10.1029/2010GL042815, 2010.
- Yoshioka, M., Mahowald, N. M., Conley, A. J., Collins, W. D., Fillmore, D. W., Zender, C. S., and Coleman, D. B.: Impact of desert dust radiative forcing on Sahel precipitation: Relative importance of dust compared to sea surface temperature variations, vegetation changes, and greenhouse gas warming, *J. Climate*, 20, 1445–1467, doi:10.1175/Jcli4056.1, 2007.
- Yu, S., Dennis, R., Roselle, S., Nenes, A., Walker, J., Eder, B., Schere, K., Swall, J., and Ro-

barge, W.: An assessment of the ability of three-dimensional air quality models with current thermodynamic equilibrium models to predict aerosol  $\text{NO}^{-3}$ , J. Geophys. Res., 110, D07S13, doi:10.1029/2004JD004718, 2005.

- 5 Zhang, J., Chameides, W. L., Weber, R., Cass, G., Orsini, D., Edgerton, E. S., Jongejan, P., and Slanina, J.: An evaluation of the thermodynamic equilibrium assumption for fine particulate composition: Nitrate and ammonium during the 1999 Atlanta Supersite Experiment, J. Geophys. Res., 107, 8414, doi:10.1029/2001JD001592, 2003.

**Optical-  
microphysical  
properties of Saharan  
dust aerosols**

A. Papayannis et al.

Title Page

Abstract

Introduction

Conclusions

References

Tables

Figures



Back

Close

Full Screen / Esc

Printer-friendly Version

Interactive Discussion



## Optical- microphysical properties of Saharan dust aerosols

A. Papayannis et al.

[Title Page](#)[Abstract](#)[Introduction](#)[Conclusions](#)[References](#)[Tables](#)[Figures](#)[⏪](#)[⏩](#)[◀](#)[▶](#)[Back](#)[Close](#)[Full Screen / Esc](#)[Printer-friendly Version](#)[Interactive Discussion](#)

**Table 1.** Percentage of mineral dust (MIN) and sulfates contribution in PM<sub>10</sub> (27 March–2 April).

Date	PM <sub>10</sub> (μg m <sup>-3</sup> )	%MIN	%SO <sub>4</sub>	%TOT(MIN + SO <sub>4</sub> )
27/3/2009	17	19.0	27.4	46.4
28/3/2009	39	18.7	13.4	32.2
28/3/2009	17	17.0	32.3	49.3
29/3/2009	17	15.1	29.4	44.5
29/3/2009	14	13.3	45.6	58.9
30/3/2009	68	34.4	16.1	50.4
31/3/2009	62	64.7	14.3	79.0
31/3/2009	62	39.8	22.2	62.0
1/4/2009	57	45.7	14.7	60.4
1/4/2009	32	78.9	17.5	96.4
2/4/2009	54	34.5	17.5	52.0

## Optical- microphysical properties of Saharan dust aerosols

A. Papayannis et al.

**Table 2.** Optical, microphysical and chemical properties of aerosols, as well as the relative humidity RH (%) at each layer, retrieved at four specific layers on 2 April 2009.

	1st layer	2nd layer	3rd layer	4th layer
Height range (km)	1.91–2.07	2.28–2.85	2.96–3.1	3.14–3.42
LR @ 355 nm (sr)	89.8 ± 0.6	89 ± 5.5	75.2 ± 0.16	76.7 ± 1.6
LR @ 532nm (sr)	64 ± 2	56.6 ± 5	47.8 ± 0.09	48.4 ± 1.9
$\hat{A}_{a355+a532}$	1.25 ± 0.008	0.935 ± 0.043	0.849 ± 0.0102	0.936 ± 0.024
Refractive Index $m_R$ (real part)	1.47 ± 0.05	1.47 ± 0.05	1.514 ± 0.05	1.52 ± 0.05
Refractive Index $m_i$ (imaginary part)	0.007 ± 0.0035	0.007 ± 0.0035	0.007 ± 0.0035	0.007 ± 0.0035
$r_{\text{eff}}$ (μm)	0.22 ± 0.06	0.32 ± 0.1	0.33 ± 0.1	0.31 ± 0.1
Surface density (μm <sup>2</sup> cm <sup>-3</sup> )	290 ± 60	210 ± 45	150 ± 30	170 ± 35
Number density (cm <sup>-3</sup> )	1700 ± 1000	1100 ± 700	700 ± 400	800 ± 500
Volume density (μm <sup>3</sup> cm <sup>-3</sup> )	21 ± 6.5	22 ± 6.5	17 ± 5	17 ± 5
RH (%)	59	64	79	80
Chemical composition	50–60 % sulfate, 15–25 % OC, 15–35 % dust	32–52 % sulfate, 28–36 % OC, 12–40 % dust	18–38 % sulfate, 52–62 % OC, 0–30 % dust	16–36 % sulfate, 54–64 % OC, 0–30 % dust

Title Page

Abstract

Introduction

Conclusions

References

Tables

Figures

⏪

⏩

◀

▶

Back

Close

Full Screen / Esc

Printer-friendly Version

Interactive Discussion

## Optical- microphysical properties of Saharan dust aerosols

A. Papayannis et al.

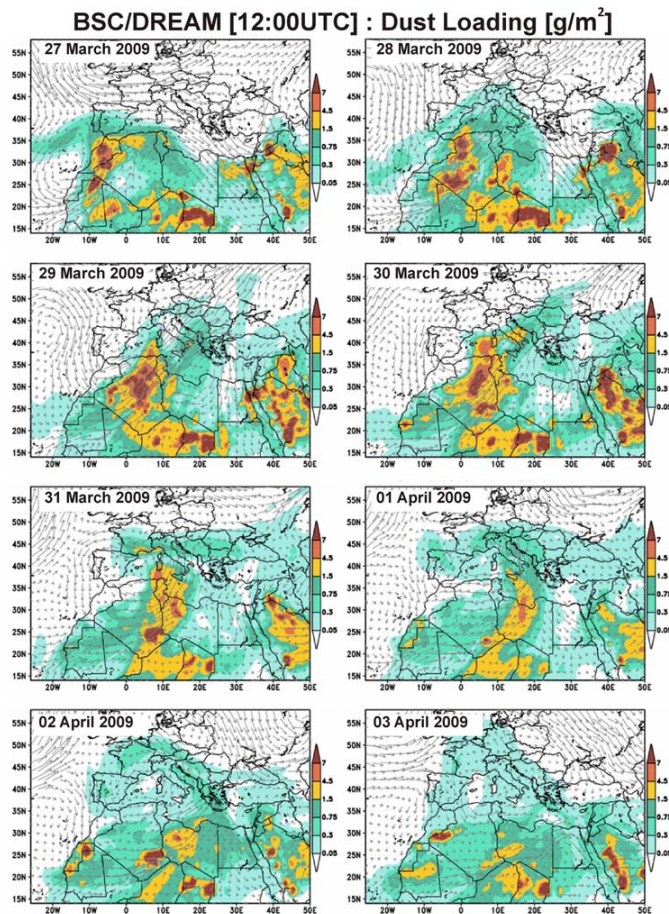


**Fig. 1.** Dust loading (in  $\text{g m}^{-2}$ ) over Europe in the period between 27 March and 3 April 2009, as estimated by the BSC-DREAM8b forecast model (12:00 UTC). The wind field pattern is also shown for 3000 m height level.

[Title Page](#)[Abstract](#)[Introduction](#)[Conclusions](#)[References](#)[Tables](#)[Figures](#)[⏪](#)[⏩](#)[◀](#)[▶](#)[Back](#)[Close](#)[Full Screen / Esc](#)[Printer-friendly Version](#)[Interactive Discussion](#)

**Optical-  
microphysical  
properties of Saharan  
dust aerosols**

A. Papayannis et al.

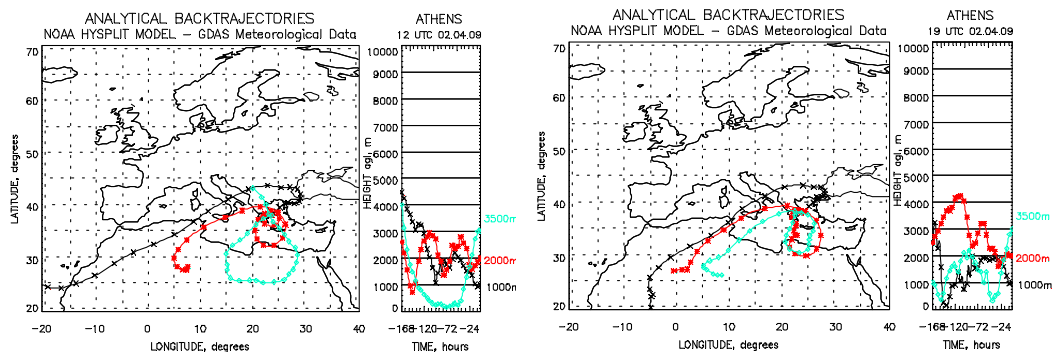


**Fig. 2.** Seven days air mass back trajectories ending over Athens on 2 April 2009 (left: at 12:00 UTC, right: at 19:00 UTC) based on the HYSPLIT model.

Title Page

Abstract

Introduction

Conclusions

References

Tables

Figures

◀

▶

◀

▶

Back

Close

Full Screen / Esc

Printer-friendly Version

Interactive Discussion

---

**Optical-  
microphysical  
properties of Saharan  
dust aerosols**A. Papayannis et al.

---

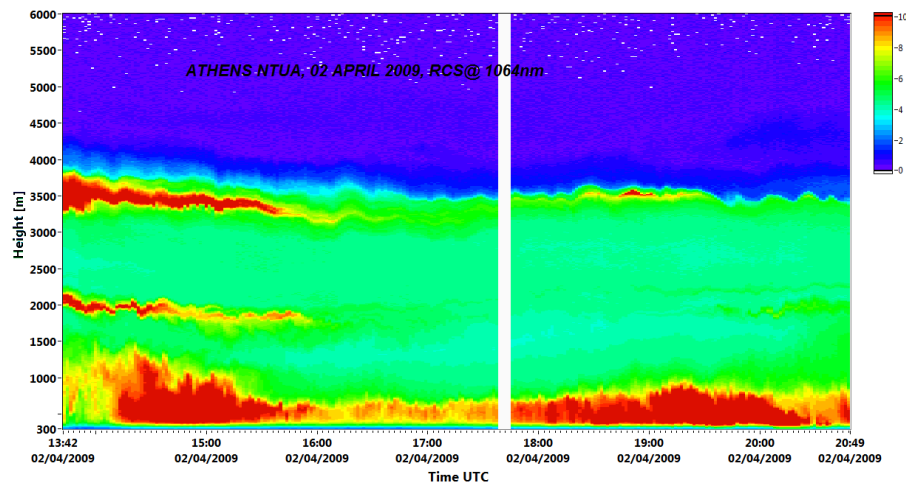


**Fig. 3.** Time-height cross section of the range-corrected backscatter lidar signal (in arbitrary units: AU) at 1064 nm, as observed over Athens, by the NTUA Raman lidar system on 2 April 2009 (13:42–20:49 UTC).

**Optical-  
microphysical  
properties of Saharan  
dust aerosols**

A. Papayannis et al.

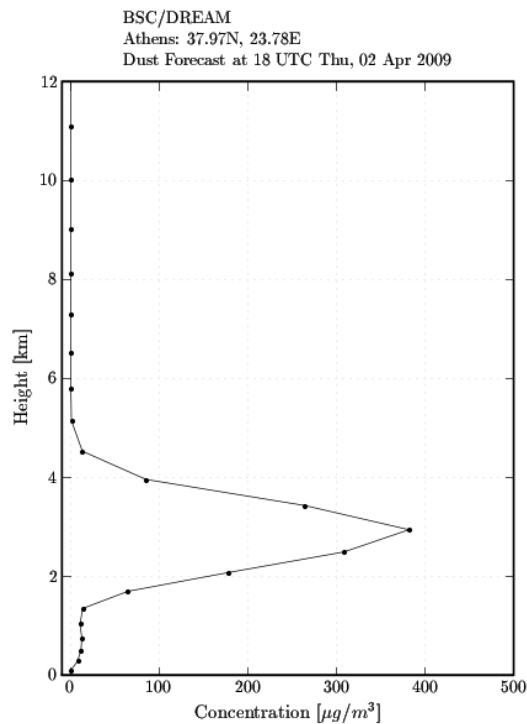


**Fig. 4.** Forecast of the vertical profile of the dust concentration (in  $\mu\text{g m}^{-3}$ ) over Athens, Greece for 2 April 2009, at 18:00 UT using the BSC-DREAM8b model.

[Title Page](#)[Abstract](#)[Introduction](#)[Conclusions](#)[References](#)[Tables](#)[Figures](#)[◀](#)[▶](#)[◀](#)[▶](#)[Back](#)[Close](#)[Full Screen / Esc](#)[Printer-friendly Version](#)[Interactive Discussion](#)

## Optical-microphysical properties of Saharan dust aerosols

A. Papayannis et al.

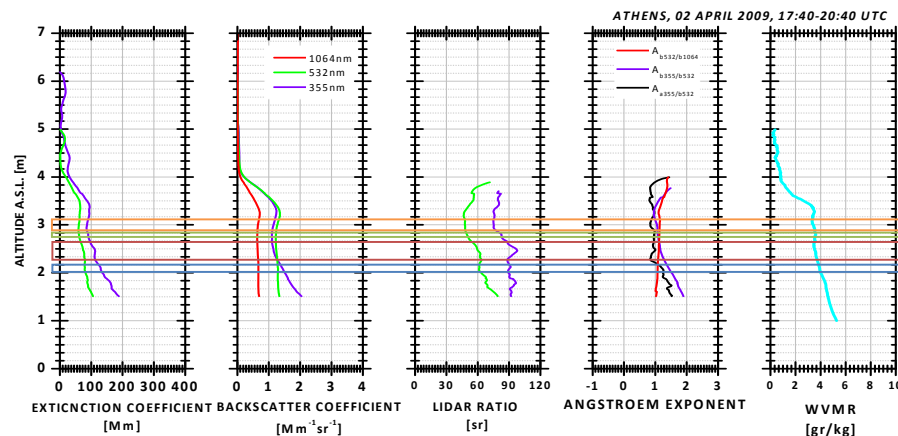


**Fig. 5.** Vertical profiles of the aerosol optical properties (extinction and backscatter coefficient, lidar ratio and Ångström backscatter and extinction-related exponent), as well as of the water vapor to dry air mixing ratio and the effective radius ( $\mu\text{m}$ ), as retrieved by the NTUA Raman lidar over Athens on 2 April 2009 (17:40–20:40 UTC).

Title Page

Abstract

Introduction

Conclusions

References

Tables

Figures



Back

Close

Full Screen / Esc

Printer-friendly Version

Interactive Discussion

## Optical- microphysical properties of Saharan dust aerosols

A. Papayannis et al.

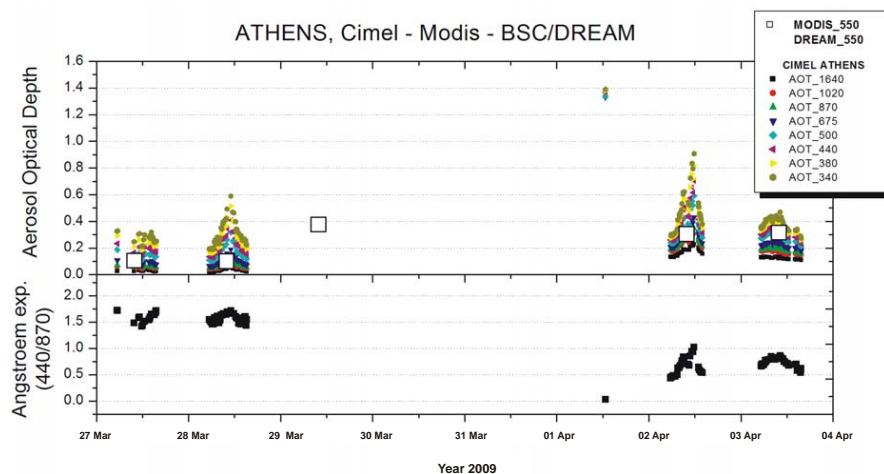


**Fig. 6.** Temporal evolution of the AOD at eight wavelengths over Athens for the period 27 March to 4 April 2009 according to CIMEL sun photometric measurements, MODIS AOD at 550 nm (white squares) and BSC-DREAM8b dust AOD at 550 nm (upper panel). Temporal evolution of the Ångström exponent (440–870 nm) for the same time period (lower panel).

Title Page

Abstract

Introduction

Conclusions

References

Tables

Figures

◀

▶

◀

▶

Back

Close

Full Screen / Esc

Printer-friendly Version

Interactive Discussion

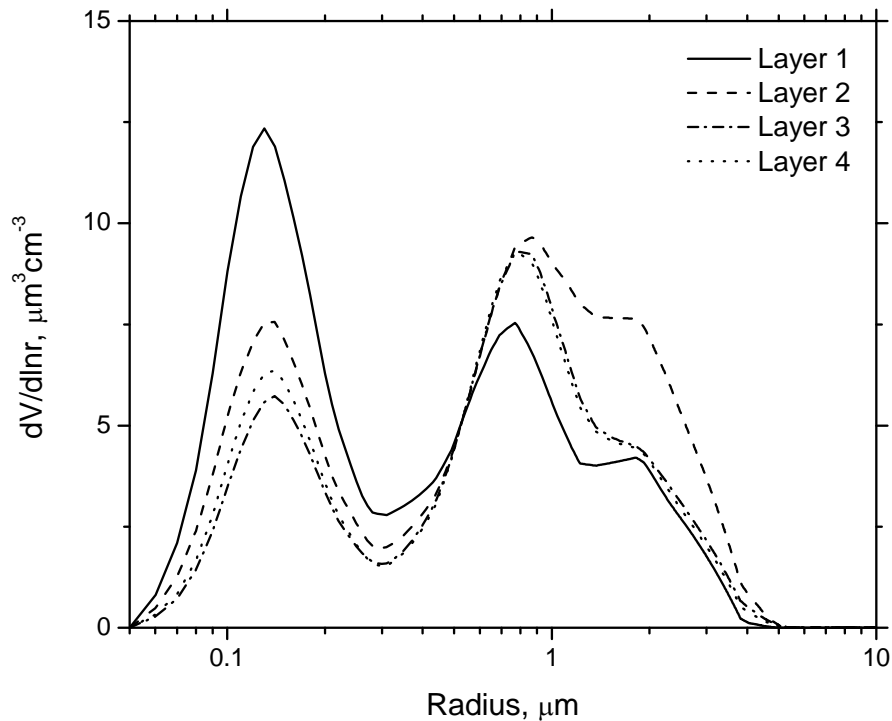


**Fig. 7a.** Retrieved aerosol volume size distribution from lidar data for diameters up to 10  $\mu\text{m}$ , for the particles in layers 1 (1910–2070 m), 2 (2284–2850), 3 (2960–3100 m) and 4 (3140–3420 km) between 17:40–20:40 UTC on 2 April 2009.

**Optical-microphysical properties of Saharan dust aerosols**

A. Papayannis et al.

Title Page

Abstract Introduction

Conclusions References

Tables Figures

⏪ ⏩

◀ ▶

Back Close

Full Screen / Esc

Printer-friendly Version

Interactive Discussion



**Optical-  
microphysical  
properties of Saharan  
dust aerosols**

A. Papayannis et al.

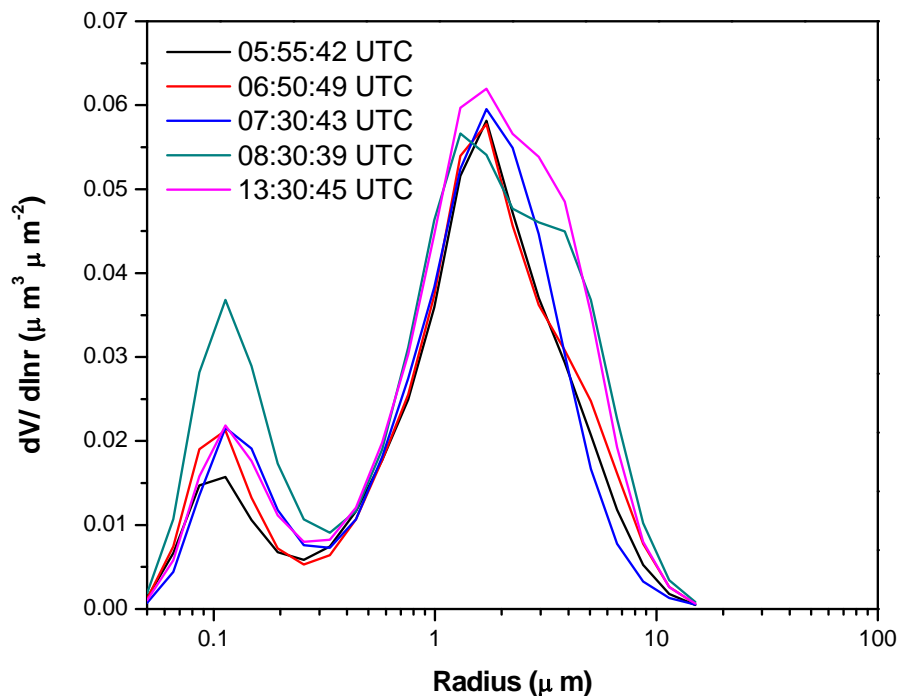


**Fig. 7b.** Left: measured aerosol volume size distribution (total column) by the CIMEL sun photometer on 2 April 2009 (from 05:55–13:38 UTC).